Edinburgh Research Explorer

New material of Chirostenotes pergracilis (Theropoda, Oviraptorosauria) from the Campanian Dinosaur Park Formation of Alberta, Canada

OPEN ACCESS

1   **New material of *Chirostenotes pergracilis* (Theropoda, Oviraptorosauria) from the**

2   **Campanian Dinosaur Park Formation of Alberta, Canada**

3

4   Funston, G. F.[1,2]*, Currie, P. J.[2]

5   *[1]School of GeoSciences, University of Edinburgh, Edinburgh, UK*

6   Grant Institute, James Hutton Road, Edinburgh, UK EH9 3FE

7   Gregory.funston@ed.ac.uk

8   *[2]Department of Biological Sciences, University of Alberta, Edmonton, AB*

9   CW 405, Biological Sciences Building, University of Alberta, Edmonton, AB T6G 2E9

10   pjcurrie@ualberta.ca

11   *Corresponding author

New material of *Chirostenotes pergracilis* (Theropoda, Oviraptorosauria) from the Campanian Dinosaur Park Formation of Alberta, Canada

Abstract:

The taxonomy of caenagnathids from the Dinosaur Park Formation of Alberta, Canada, has remained problematic because of incomplete, partial skeletons that do not overlap anatomically. This is particularly problematic for referring mandibular remains, which are the most abundant caenagnathid fossils recovered, but cannot be confidently tied to taxa known from postcranial remains. A new, partial skeleton of *Chirostenotes pergracilis* preserves the mandibles, cervical and caudal vertebrae, and parts of the hindlimb. Importantly, this is the first specimen with associated mandibles and postcrania of a caenagnathid from the Dinosaur Park Formation, allowing for unambiguous referral of mandibles to this taxon. The mandibles are remarkably similar to those previously suggested to pertain to *Chirostenotes pergracilis*, and support its distinction from *Caenagnathus collinsi*. An unfused distal tarsal IV distinguishes the skeleton from *Leptorhynchos elegans* and supports the referral of small, upturned mandibles to this taxon. Osteohistological analysis indicates that the individual was approaching maximum body size, and provides information on the growth patterns and size of *Chirostenotes pergracilis*. Accordingly, this supports the division of Dinosaur Park Formation caenagnathids into three taxa of varying body sizes.

Keywords:

Caenagnathidae; Oviraptorosauria; Late Cretaceous; Osteohistology; Dinosaur Park Formation.

Introduction:

Caenagnathidae is a clade of maniraptoran theropods from the Cretaceous of Asia and North America. The first known caenagnathid, *Chirostenotes pergracilis*, was named by Gilmore (1924) based on an articulated manus from the Upper Cretaceous (Campanian) Dinosaur Park Formation (DPF) of Alberta, Canada. Other caenagnathid material was described, mostly as new taxa, by C.M. Sternberg (1932; 1934), Parks (1933), and R.M. Sternberg (1940), although it was not clear until much later that this material pertained to the same group as *Chirostenotes pergracilis* (Osmólska 1976; Osmólska 1981; Currie 1989). A partial skeleton of *Chirostenotes pergracilis* including most of the hindlimb was described by Currie and Russell (1988). Its metatarsal structure suggested to Currie and Russell (1988) that *"Macrophalangia canadensis"* (Sternberg 1932) was the junior synonym of *Chirostenotes pergracilis.* Currie (1989) noticed similarities between the small, fused tarsometatarsus of *'Ornithomimus' elegans* (Parks 1933) and those of *Elmisaurus rarus* (Osmólska 1981) from Mongolia. He suggested they were congeneric, and that *Elmisaurus elegans* and *Chirostenotes pergracilis* could be distinguished by fusion of the tarsometatarsus (Currie 1989). However, this was complicated by a partial skeleton (ROM 43250) from the Horseshoe Canyon Formation of Alberta, described by Sues (1997). Although the specimen cemented the synonymy of Caenagnathidae and Elmisauridae (Sues 1997), it stimulated debate about which specimens were conspecific. Whereas Currie (1989) preferred to separate DPF caenagnathid material from into three genera: *Caenagnathus*, *Chirostenotes*, and *Elmisaurus*, Sues (1997) argued that all of this material should be united. Later, Sullivan et al. (2011) suggested, on the basis of stratigraphic separation, that the material described by Sues (1997) was distinct enough to merit a new name: *Epichirostenotes curriei.*

56　Taxonomic separation of ROM 43250 from *Chirostenotes pergracilis* called into question the

57　assertion of Sues (1997) that *Caenagnathus collinsi*, *Chirostenotes pergracilis*, and *Elmisaurus*

58　*elegans* were synonymous. Accordingly, most studies now follow Currie (1989) in the separation

59　of DPF caenagnathids into three taxa (Longrich et al. 2013; Lamanna et al. 2014; Funston &

60　Currie 2016).

61　　　In the last fifteen years, a number of new discoveries have ameliorated our understanding

62　of the diversity and anatomy of caenagnathids, especially in Asia. Xu et al. (2007) described the

63　appropriately named *Gigantoraptor erlianensis* on the basis of a giant skeleton from China with

64　clear oviraptorosaur affinities. Subsequent cladistic analyses (Lamanna et al. 2014; Funston &

65　Currie 2016) have placed *Gigantoraptor* as a basal caenagnathid, mostly on the basis of the

66　mandible. Ma et al. (2017) further described the mandible of *Gigantoraptor* in more detail, and

67　assessed the functional morphology of its intermediate shape. Sues and Averianov (2015)

68　described additional material of the miniscule *Caenagnathasia martinsoni*, including vertebrae

69　and a femur. Yao et al. (2015) described another partial mandible of *Caenagnathasia*, but from

70　the Iren Dabasu Formation of China, expanding the stratigraphic and geographic range of

71　*Caenagnathasia.* Tsuihiji et al. (2015) described a pair of giant mandibles from the Bayn Shiree

72　Formation of Mongolia, noting similarities to *Gigantoraptor erlianensis*. The same authors then

73　described much smaller, fused dentaries probably referable to *Elmisaurus rarus* from the Nemegt

74　Formation exposed at Bugiin Tsav (Tsuihiji et al. 2016). Pu et al. (2017) published the long-

75　awaited description of 'Baby Louie' from Henan Province in China, interpreting it as a new,

76　giant caenagnathid closely related to *Gigantoraptor erlianensis*. Recently, Yu et al. (2018)

77　named an intermediately-sized caenagnathid, *Anomalipes zhaoi*, from the Late Cretaceous of

78　China, filling the former gap in body sizes of Chinese caenagnathids between *Caenagnathasia*

and *Gigantoraptor*. Wang et al. (2017; 2018) argued, based on tooth-loss patterns in a Jurassic ceratosaur and the Early Cretaceous bird *Sapeornis*, that caenagnathids underwent ontogenetic edentulism. On this basis, they argued that the complex structures on the occlusal surfaces of the dentaries were the vestiges of tooth-bearing structures. However, this finding was contested by Funston et al. (2019), who used osteohistology to show that caenagnathid dentaries lacked any evidence of tooth-bearing tissues. These studies have shown that caenagnathids were diverse and broadly distributed in the Late Cretaceous, but they have done little to clarify the taxonomy or relationships of the group.

However, better material from North America has provided some advances on this front. Lamanna et al. (2014) described *Anzu wyliei*, the largest caenagnathid known from North America, from three reasonably complete skeletons from the Upper Cretaceous (Maastrichtian) Hell Creek Formation. These specimens show that *Anzu* had a prominent cranial crest and a short tail with modified pygostyle-like distal vertebrae. Importantly, these specimens also provide concrete evidence that caenagnathid mandibles and postcrania pertain to the same animals. Funston and Currie (2016) described a relatively complete skeleton of a new taxon, *Apatoraptor pennatus*, from the Horseshoe Canyon Formation, which helped to resolve some aspects of caenagnathid phylogeny. Although less complete, numerous new caenagnathid specimens have also been described from the DPF (Longrich et al. 2013; Funston & Currie 2014; Bell et al. 2015; Funston et al. 2015; Funston, Currie, & Burns 2016; Gregory F. Funston et al. 2019), and these help to improve our understanding of the anatomy and variation in caenagnathids.

Regardless of this considerable progress, the taxonomy of DPF caenagnathids has remained obscure and unresolved. This is due in large part to the fragmentary, non-overlapping nature of partial skeletons known thus far from the DPF—in spite of producing the greatest

102 abundance of caenagnathid specimens globally. Nonetheless, this issue remains central to

103 unravelling the relationships and ecology of caenagnathids. Confident referral of isolated DPF

104 specimens to their respective taxa would greatly improve skeletal representation and

105 phylogenetic character scores.

106   In 2016, a partial caenagnathid skeleton (UALVP 59400) was found in the southeastern

107 part of Dinosaur Provincial Park (Fig. 1). The specimen comprises a relatively complete

108 mandible and elements of the axial and appendicular skeleton, providing the first associated

109 mandibular and postcranial material from the DPF. The morphology of the mandible and a distal

110 tarsal IV indicate that this specimen is attributable to *Chirostenotes pergracilis*. In addition,

111 reexamination suggests that some previously collected material can also be referred to

112 *Chirostenotes pergracilis* on the basis of overlap with known specimens. These specimens are

113 described here with osteohistological analyses to assess relative maturity of the individual

114 represented by UALVP 59400. The new material helps to resolve some of the ambiguities

115 regarding taxonomy and diversity of DPF caenagnathids, and provides some insights into the

116 growth patterns of *Chirostenotes pergracilis*.

117 ***Institutional Abbreviations:***

118 **CMN**, Canadian Museum of Nature, Ottawa, ON, Canada; **TMP**, Royal Tyrrell Museum of

119 Palaeontology, Drumheller, AB, Canada; **UALVP**, University of Alberta Laboratory for

120 Vertebrate Palaeontology, Edmonton, AB, Canada.

121

122 **Materials and Methods:**

123

The material was excavated under provincial and parks collecting permits to PJC (UALVP
59400) or the TMP. UALVP 59400 consisted of several badly crushed blocks that developed
fracture planes through the bones. Because of the delicate nature of the specimen, the unprepared
blocks were CT scanned using a Siemens Sensation 64 Medical CT scanner and visualized using
Mimics 14.0 to guide preparation. The blocks were then mechanically prepared using
conventional methods and photographed using a Nikon D7200 digital camera. Photographs were
processed using Adobe Photoshop CC or Adobe Photoshop 2020. Any adjustments made to
brightness, contrast, or colour balance were applied to the whole image. Osteohistological thin-
sections of UALVP 59400 were made by vacuum-embedding a fragment of an indeterminate
long bone in Castolite AC polyester resin, and cutting the billet using an Isomet 1000 Precision
Sectioning Saw. Billets were adhered to plexiglass slides using 3M Cyanoacrylate glue. The
mounted billet was resectioned to a thickness of 0.7mm, and then ground and polished by hand
using 600-grit powder on a glass plate. The slides were polished on a buffing pad and mineral oil
was applied to enhance optical clarity. Slides were imaged under plane polarized and cross-
polarized light using NIS Elements on a Nikon Eclipse E600POL trinocular polarizing
microscope with an attached Nikon DXM 1200F digital camera. For enhanced clarity and depth
of field, some pictures (both microscopic and macroscopic) were generated using Z-stacked
images. These were created manually, using either NIS Elements or Adobe Photoshop 2020.

Systematic Palaeontology:

<div align="center">

DINOSAURIA Owen, (1842)

SAURISCHIA Seeley, (1888)

</div>

147   THEROPODA Marsh, (1881)

148   COELUROSAURIA von Huene, (1914)

149   MANIRAPTORA Gauthier, (1986)

150   OVIRAPTOROSAURIA Barsbold, (1976)

151   CAENAGNATHIDAE R. M. Sternberg, (1940)

152   *CHIROSTENOTES PERGRACILIS* Gilmore, (1924)

153   *Holotype:*

154   CMN 2367, articulated manus (Gilmore, 1924)

155   *Referred Material:*

156   CMN 8538, right pes (Sternberg 1932); TMP 1979.020.0001, partial skeleton (Currie and

157   Russell 1988); TMP 1985.043.0070, partial dentaries (Gregory F. Funston et al. 2019); TMP

158   1992.036.1237 (Gregory F. Funston et al. 2019); TMP 2001.012.0012, complete mandibles

159   (Funston & Currie 2014).

160   *Newly Referred Material:*

161   TMP 1990.056.0006, fused dentaries; TMP 1996.036.0181, partial tarsometatarsus (Funston,

162   Currie, & Burns 2016); TMP 2002.012.0103, partial ilium; UALVP 59400, partial skeleton

163   (GPS: UTM 12U 468540, 5621530).

164   *Locality and Horizon:*

165   Dinosaur Park Formation (Campanian), Dinosaur Provincial Park, Alberta, Canada (Fig. 1).

166   *Revised Diagnosis* **(modified from Currie and Russell 1988 and Longrich et al. 2013)***:*

167   Medium-sized (~65 kg) caenagnathid oviraptorosaur diagnosed by the following autapomorphies

168   (*) and combination of characters: occlusal tip of dentary upturned at approximately 45°*;

169   dentaries fused with well-developed symphyseal shelf; deep mandibular fossa; dentary excluded

170   from dorsal margin of external mandibular fenestra by surangular; articular ridge of mandible

171   distinctly offset from dorsal margin of surangular; cervical vertebrae with low neural spines and

172   small epipophyses; six sacral vertebrae with pleurocoels; distal caudal vertebrae with anteriorly-

173   directed transverse processes; posterior chevrons anteroposteriorly elongate at proximal end, as

174   long or longer anteroposteriorly than corresponding caudal vertebrae*; digit III of manus longer

175   than digit I, but with slender phalanges; tall, dolichoiliac ilium with reduced postacetabular

176   blade*; distal tarsals and proximal metatarsals not coossified at maturity; metatarsal III

177   proximally pinched between metatarsals II and IV, but only the proximal tip is excluded from the

178   anterior surface of the metatarsus; metatarsal V strongly procurving and not fused to distal tarsal

179   IV*.

180   **Description:**

181

182   ***UALVP 59400:***

183   UALVP 59400 (Table 1) consists of a partial articulated skeleton including the mandible, four

184   cervical vertebrae, eleven caudal vertebrae and associated chevrons, a partial pubis and ischium,

185   fragments of a femur and tibia, both astragali, and a right distal tarsal IV (Fig. 1C). The bones are

186   transversely crushed but otherwise relatively well preserved.

187   *Mandible:*

188   The mandible (Fig. 2) is relatively complete, consisting of badly crushed, fused dentaries and

189   portions of both articular-surangular-coronoid (ASC) complexes. The angulars are preserved as a

190   collection of fragments that likely represent a significant proportion of the bones, but cannot be

191   reconstructed. The left dentary is more complete and can be rearticulated with the corresponding

192   ASC complex (Fig. 2A–D), which is less complete than that of the right side (Fig. 2E–J). The

193   mandible is overall remarkably similar to TMP 2001.012.0012 in morphology, but it is slightly

194   smaller in size. The dentary is transversely crushed but still preserves much of the morphology.

195   The anterior occlusal grooves and ridges are shallow and lack nodules, in contrast to TMP

196   1992.036.0390. There are four lateral occlusal ridges (Fig. 2C, D), which become successively

197   smaller posteriorly. They border a deep lingual groove, which itself lies lateral to the well-

198   developed lingual ridge. The tubercle of the lingual ridge is distorted by crushing, but it does not

199   appear to have been as prominent as that of TMP 1992.036.1237, nor does it have the small

200   nodules present in the latter. The symphyseal sulcus is mostly missing. The lateral surface of the

201   dentary is pierced by numerous foramina (Fig. 2A, B), which, as in TMP 2001.012.0012, are

202   arranged into three rows (Funston and Currie 2014). A mandibular fossa is present and

203   apparently deep, but it is deformed by transverse and dorsoventral crushing. The ventral surface

204   of the dentary is only preserved at its posterior end, near the attachment of *M. genioglossus*. This

205   scar is roughly heart-shaped and foramina demarcate its posterior border. The Meckelian grooves

206   converge towards the midline, and open posteroventrally on the posteromedial surface of the

207   dentary. The rami of the dentaries bifurcate around a large external mandibular fenestra. The

208   dorsal ramus is strap-like and forms an interfingering joint with the ASC complex (Currie et al.

209   1993; Funston & Currie 2014). The ventral ramus tapers posteriorly and lies lateral to the

210   angular, which has a deep groove for this contact. The ASC complex has a rugose, medially

211   deflected coronoid process, which, as in TMP 2001.012.0012 (Funston & Currie 2014), has a

212   distinct ventral suture (Fig. 2E, F). A small foramen pierces the medial surface of the surangular

213   near its contact with the angular, but this does not form a fenestra in the way that it does in

214   oviraptorids. The articular has a tall median ridge that presumably was flanked by tongue-like

215   medial and lateral cotyles as in TMP 2001.012.0012, although these are missing in UALVP

216   59400. The slope of the anterior part of the articular ridge, where it meets the surangular, is less

217   steep than in TMP 2001.012.0012, but it is more pronounced than in *Anzu wyliei* (Lamanna et al.

218   2014) and *Caenagnathus collinsi* (Currie et al. 1993). It is most similar to that of *Apatoraptor*

219   *pennatus* (Funston and Currie 2016).

220   *Cervical Vertebrae:*

221   Four cervical vertebrae are preserved, three of which are still in articulation (Fig. 3). Two mid-

222   cervical vertebrae, probably representing postaxial cervical vertebrae 7–8 based on comparison

223   to *Apatoraptor pennatus*, are better preserved. The morphologies of their centra are difficult to

224   discern, but the neural arches are well preserved. The neurocentral suture is obliterated in all of

225   the vertebrae. The centrum of the anterior vertebra appears to have a longitudinal ridge

226   underlying the infrapostzygapophyseal fossa on the neural arch (Fig. 3). Ventral to this, there is a

227   large lateral pleurocoel that opens posteriorly. The diapophysis is connected to the

228   postzygapophysis by a broad lamina that forms the dorsal edge of the infrapostzygapophyseal

229   fossa. The neural spine is dorsoventrally short and rounded in lateral view (Fig. 3). The

230   postzygapophysis faces ventrally and the epipophysis is small or absent. The posterior cervical

231   vertebra preserves the entire neural arch, but it is more damaged than the anterior one. The

232   prezygapophysis is upturned, which may be taphonomically modified, although it also appears to

233   be the case in postaxial cervical vertebra eight of *Apatoraptor pennatus* (Funston and Currie

234   2016). The neural spine is low and rounded. The postzygapophyses face ventrally and also seem

235   to lack epipophyses. Like the anterior vertebra, the neural arch has a broad lamina that connects

236   the postzygapophysis to the diapophysis. The diapophysis is apparently fused to the cervical rib,

237   although this region is damaged and the fusion cannot be determined without doubt. Dorsal to

238   the two better preserved cervical vertebrae is a patch of matrix with filamentous stains (Fig. 3).

239   There is a distinct 'tufted' border between these stains and the matrix further away from the

240   specimen, and the filaments appear to have a consistent orientation extending posterodorsally

241   from the vertebrae. Most filaments preserved in this region are approximately 1 mm long and

242   vary considerably in thickness. However, many of these filaments appear to form continuous,

243   parallel lines that can be as long as 1 cm (Fig. 3C–E). The colouration of the filaments varies

244   from black to dark brown to a rusty orange or red colour. Filaments of these various colours are

245   interspersed in the same regions, creating a speckled pattern (Fig. 3C). The most posterior patch

246   of impressions (Fig. 3E) has the highest proportion of black filaments, and these are generally

247   arranged into parallel rows of smaller filamentous specks. Two predominant orientations of these

248   rows can be discerned, one extending posterodorsally, and one extending anteroposteriorly.

249   Some possible branching structures can be discerned close to the vertebra (Fig. 3E), but these

250   may simply be patchy preservation of the filamentous stains.

251   *Caudal Vertebrae:*

252   A series of thirteen articulated caudal vertebrae (Figs 4, 5) were preserved with the skeleton, of

253   which eleven remained in one block. The caudal vertebrae likely represent the penultimate part

254   of the tail, and do not include the pygostyle. This is evident from the positions of the neural

255   spines posterior to the articular faces of the corresponding vertebrae and the anteriorly directed

256   transverse processes on the most posterior caudal vertebrae (Fig. 5). The more anterior caudal

257   vertebrae (Fig. 4) have barrel-shaped centra with large lateral pleurocoels, which decrease in size

258   posteriorly along the tail (Table 1). In the posterior caudal vertebrae, these pleurocoels are slit-

259   like, underlying the infradiapophyseal fossa, and they are absent in the last three caudal

260   vertebrae. The neural spines are low and triangular in lateral view. The transverse processes are

261   elliptical in cross section, tongue-like in dorsal view, and extend posterolaterally in the anterior

262   caudal vertebrae (Fig. 4). Posteriorly, the transverse processes become more platelike, taper at

263   their lateral ends, and become successively more anteriorly directed. In the anterior caudal

264   vertebrae, there is a well developed infradiapophyseal fossa and a smaller infraprezygapophyseal

265   fossa, but the presence of an infrapostzygapophyseal fossa cannot be determined because this

266   area is overlain by the fingerlike prezygapophyses. The last two caudal vertebrae are slightly

267   disarticulated and lie nearly perpendicular to the rest of the series (Figs. 4, 5). The centra of these

268   vertebrae are transversely wider than they are dorsoventrally tall, and they have a groove along

269   the ventral midline (Fig. 5). The transverse processes extend from the widest point of the

270   centrum and curve anteriorly from their bases. In these respects, they are similar to the

271   penultimate caudal vertebrae of *Nomingia gobiensis* (RZNCHEN Barsbold et al. 2000), and they

272   likely represent the corresponding vertebrae. Specifically, the last caudal vertebra preserved with

273   UALVP 59400 is nearly identical to caudal vertebra 17 of *Nomingia gobiensis* (Rinchen

274   Barsbold et al. 2000). If this is the case, only four additional vertebrae would be missing from the

275   anterior part of the caudal vertebral series, and seven from the posterior part of the tail.

276   *Chevrons:*

277   The chevrons (Fig. 6) are exceptionally large compared to other oviraptorosaurs, especially

278   considering the distal positions of the corresponding caudal vertebrae. Anteriorly, the chevrons

279   are elongate and taper towards their rounded distal ends. Posteriorly, they become dorsoventrally

280   shorter and more platelike (Fig. 4), but do not decrease in anteroposterior length. The result is

281   that the proximal ends of the posterior chevrons are nearly in contact, and the most posterior

282   chevrons are longer anteroposteriorly than their corresponding vertebrae. A similar morphology

283   is present in *Nomingia gobiensis* (RZNCHEN Barsbold et al. 2000), but not to the same extreme

284   as in UALVP 59400.

285   *Pelvis:*

286   Small portions of a pubis and ischium (Fig. 7) are represented by fragments collected as float. A

287   single fragment of the pubis is from the proximal end where it would have contacted the ilium

288   and provides no information. The ischium is better represented, and most of a shaft can be

289   reconstructed, although it is likely some fragments are from opposite sides. The reconstructed

290   morphology of the ischium (Fig. 7) is similar overall to that of TMP 1979.020.0001 in that it is

291   posteriorly concave and has a tab-like obturator process.

292   *Hindlimb:*

293   The hindlimb is known from fragments of the femur and/or tibia, both astragalocalcanea (Fig. 8),

294   and a distal tarsal IV (Fig. 9). It is likely that some of the float fragments pertain to other

295   hindlimb bones including metatarsals, but these cannot be identified with certainty. Based on the

296   curvature of some fragments, they may represent the femur and/or tibia, but they do not provide

297   any morphological information. The distal end of the right tibia is preserved in articulation with

298   the badly crushed astragalocalcaneum (Fig. 8). All that can be said of these is that they were not

299   fused, the postfibular flange of the tibia was small, and the astragalocalcaneum extended onto the

300   posterior surface of the tibia as in CMN 8538. The left astragalocalcaneum is less crushed and

301   shows that there was a transverse groove above the distal condyles (Fig. 8), as in other DPF

302   caenagnathids (Currie & Russell 1988; Funston et al. 2015), rather than a median tubercle as in

303   *Anzu wyliei* (Lamanna et al. 2014). The right distal tarsal IV (Fig. 9) is well preserved and

304   relatively complete. It is roughly triangular in proximal view and tapers in proximodistal

305   thickness towards its anterior edge. The proximodorsal process is broken off, but posterior to it

306   there is a notch for metatarsal V (Fig. 9F), which contrasts the morphology of fused

307   tarsometatarsi referable to *Leptorhynchos elegans* (Currie 1989; Funston, Currie, & Burns 2016).

308 In *Leptorhynchos elegans*, metatarsal V contacts and fuses with the proximodorsal process, and

309 this coossification fills the notch for metatarsal V . The medial edge of the distal tarsal is mostly

310 broken, but some intact surface indicates that this tarsal was not fused to distal tarsal III, which

311 occurs in *Elmisaurus rarus* and *Leptorhynchos elegans* (Osmólska 1981; Currie 1989; Currie et

312 al. 2016; Funston, Currie, & Burns 2016). Similarly, the intact ventral (distal) articular surface

313 (Fig. 9D) indicates that distal tarsal IV had not fused to the proximal metatarsus, despite

314 histological maturity of this individual (see subsequent discussion). This strongly suggests that

315 this individual did not have a proximally fused metatarsus, which contrasts with all known

316 specimens of *Leptorhynchos elegans* (Currie 1989; Funston, Currie, & Burns 2016), but is

317 similar to the known specimens referred to *Chirostenotes pergracilis* (Sternberg 1932; Currie &

318 Russell 1988; this study).

319

320 ***TMP 1993.036.0181:***

321 TMP 1993.036.0181 (Fig. 10) is a pathological, partial tarsometatarsus described by Funston et

322 al. (2016), and includes metatarsals II and IV and distal tarsals III and IV. Although initially

323 described as a representative of *Leptorhynchos elegans* (Funston, Currie, & Burns 2016), several

324 features suggest it more likely represents *Chirostenotes pergracilis*. For example, it is the largest

325 tarsometatarsus recovered from Alberta (~250 mm), comparable in size with the holotype of

326 "*Macrophalangia*", CMN 8538 (Sternberg 1932), but is not proximally coossified. This is most

327 evident in the absence of the proximal end of metatarsal III, which shows it had not coossified,

328 whereas metatarsal III is fused with metatarsals II and IV in all known individuals of

329 *Leptorhynchos elegans* (Currie 1989; Funston, Currie, & Burns 2016). The clean contact

330 surfaces for metatarsal III on the proximal ends of metatarsals II and IV further demonstrate the

331   lack of coossification in this individual. Upon reexamination, it is clear that the distal tarsals are

332   not coossified to each other or with the metatarsals, and a clear suture is visible between them

333   (Fig. 10). This contrasts with *Leptorhynchos elegans*, where the distal tarsals fuse to each other

334   and the proximal metatarsus (Currie 1989; Funston, Currie, & Burns 2016). The absence of

335   fusion between metatarsal V, which is missing, and the proximodorsal process of distal tarsal IV

336   also contrasts with the condition in known specimens of *Leptorhynchos elegans* (Funston,

337   Currie, & Burns 2016). In their initial description of the specimen, Funston et al. (2016) also note

338   that the muscle scars for *M. tibialis cranialis* are less well developed in TMP 1993.036.0181 than

339   in most specimens of *Leptorhynchos elegans*. In all of these features, TMP 1993.036.0181

340   closely resembles *Chirostenotes pergracilis* (CMN 8538 and TMP 1979.020.0001).

341

342   ***TMP 2002.012.0103:***

343   TMP 2002.012.0103 is a partial right ilium (Fig. 10A–C) that includes the postacetabular blade

344   and acetabulum. The pubic peduncle is incompletely preserved, but its ventral edge is

345   distinctively inclined anterodorsally, similar to TMP 1979.020.0001 but not other DPF

346   caenagnathid ilia. The acetabulum is slightly constricted transversely at its anteroposterior

347   midpoint (Fig. 10C), but not to the same degree as other oviraptorosaurs. The ischiadic peduncle

348   is small and triangular, extending to the same level ventrally as the pubic peduncle. Two large

349   foramina pierce the posterior surface of the ischiadic peduncle. The postacetabular blade has a

350   curved dorsal edge, similar to TMP 1979.020.0001, although it is broken along most of its

351   length. There is a region of rugose bone near the ventral edge of the postacetabular blade that

352   probably anchored musculature. The medial surface of the ilium (Fig. 10B) is excavated by three

353   deep concavities, ventral to which a platform accommodates the sacral rib attachments. The

354 brevis fossa is shallow but the brevis shelf is broken, so its full extent cannot be determined.

355 Overall the morphology of the ilium is remarkably similar to TMP 1979.020.0001, although

356 TMP 2002.012.0103 is slightly larger and more robustly built.

357

358 **Osteohistology**

359 A fragment of an indeterminate long bone (probably the femur or the tibia) was thin-sectioned to

360 assess the histological maturity of UALVP 59400 (Fig. 11). The element represented by the

361 fragment cannot be determined with certainty, but considering its featureless external surface and

362 the curvature of the fragment, it probably represents an area close to the midshaft of either the

363 femur or the tibia. Other long bones, like the forelimb bones or metatarsals, have smaller

364 diameters than the femur and tibia (Currie & Russell 1988), and thus would be expected to show

365 tighter curvature than in this fragment. The exact position of the fragment relative to the midshaft

366 cannot be established, which limits its usefulness for skeletochronology (Padian et al. 2013), but

367 it clearly preserves some of the growth record and has little external evidence of muscular

368 attachment. Because of the limited nature of the material available for sampling, only very

369 limited insights can be made regarding the growth of this individual (Horner et al. 1999; Horner

370 et al. 2001; Cullen et al. 2014; Woodward et al. 2014; Woodward et al. 2015). However, this

371 information is nonetheless important for our understanding of caenagnathid diversity in the DPF.

372 Future systematic study of caenagnathid osteohistology using better material may provide a more

373 complete context within which UALVP 59400 can be placed.

374 Histological preservation of the specimen is excellent and several important features can

375 be discerned (Fig. 11). The relative bone wall thickness is low, as expected of a theropod

376 (Varricchio 1993; Horner & Padian 2004; Erickson et al. 2009; Funston, Currie, & Burns 2016),

377   but its exact value cannot be calculated without more complete material, as there is uncertainty in

378   the diameter of the bone. The medullary cavity is large and lined by thick layers of endosteal

379   lamellae (Fig. 11B), which suggests much of the earlier growth record has been resorbed (Horner

380   & Padian 2004; Padian et al. 2013). There are no trabeculae in the medullary cavity, which is

381   similar to other theropods (Varricchio 1993; Horner & Padian 2004; Cullen et al. 2014; Xu et al.

382   2018). The cortex is composed of mostly of primary fibrolamellar bone (Francillon-Vieillot et al.

383   1990) with abundant vascularization. Osteocyte lacunae are relatively dense ($\sim$ 47,000/mm^3),

384   similar to other oviraptorosaurs and small dinosaurs (Stein & Werner 2013; Cullen et al. 2014;

385   Funston & Currie 2018; Gregory F. Funston et al. 2019). Most osteocytes are flattened in shape,

386   reflecting the well-developed primary osteons and the accompanying lamellar bone. The density

387   and shape of the osteocytes is consistent throughout the entire cortex. Vascularity throughout the

388   cortex is predominantly reticular in orientation, but in some areas of the inner cortex, it

389   approaches a sub-plexiform orientation (Fig. 11E). Conversely, towards the periosteal surface

390   there is a higher proportion of longitudinal canals (Fig. 11E). In these regions, the bone

391   approaches a laminar organization (Francillon-Vieillot et al. 1990). Regardless, many radial

392   anastomoses are still present in this region, and in most areas the vascularity is best described as

393   reticular (Francillon-Vieillot et al. 1990; de Margerie 2004).

394   The cortex is marked by 11 lines of arrested growth (LAGs), two pairs of which are

395   doublet LAGs (Fig. 11C)—common in non-avian theropods (Lee & O'Connor 2013; Cullen et

396   al. 2014; Zanno et al. 2019). These doublet LAGs likely represent a single cyclical growth mark

397   (CGM; Castanet et al. 1990), and taking this into consideration, nine CGMs can be counted

398   throughout the cortex (Fig. 11E). Whereas the outer LAGs are each roughly parallel to the

399   endosteal and periosteal surfaces, the innermost LAG is more tightly curved and intersects with

400 the medullary cavity at one end. Each LAG is accompanied endosteally by an annulus of bone

401 with an increased proportion of parallel-fibered bone matrix and a reduction in vascularity (Fig.

402 11D). An extra annulus can be discerned periosteal to the innermost LAG, but it does not

403 encircle the entire cortex, nor is it associated with a rest line. The CGMs decrease in spacing

404 towards the periosteal surface, but not in a regular fashion. Whereas the first, second and third

405 CGMs are widely spaced, the remaining CGMs are much more closely spaced (Fig. 11E). These

406 more periosteal CGMs are evenly spaced, each separated by a single circumferential row of

407 predominantly longitudinal vascular canals (Fig. 11E). The close packing of LAGs and annuli

408 towards the periosteal surface is associated with a higher proportion of parallel-fibered bone

409 matrix (Fig. 11D), but the matrix is still predominantly fibrolamellar. These LAGs therefore do

410 not represent a fully-developed external fundamental system (Horner et al. 1999; Woodward et

411 al. 2014; Woodward et al. 2015). However, the bone right at the periosteal surface is parallel-

412 fibered and has reduced vascularity (Fig. 11D), which suggests it may represent an incipient

413 EFS. Alternatively, this may represent the formation of the annulus that precedes LAGs

414 elsewhere in the cortex. Secondary remodelling is generally restricted, but there are some

415 secondary osteons endosteal to the innermost LAG (Fig. 11B). These are concentrated in a small

416 area and none are cross-cut by other secondary osteons, nor by the endosteal lamellae.

417

418 **Discussion:**

419

420 *Taxonomy:*

421 A complete taxonomic review is beyond the scope of this study and is in preparation for

422 publication elsewhere (GFF in prep). However, it is important to note that where DPF

423   caenagnathid elements are known from multiple specimens (i.e. mandibles, ilia, tarsometatarsi),

424   in each case they support the distinction of only three morphotypes—likely corresponding to the

425   three currently recognized genera. In addition to morphology, these groups appear to differ in

426   adult body size (Bell et al. 2015; Funston et al. 2015; Gregory F. Funston et al. 2019), and

427   currently known material from *Chirostenotes pergracilis* is intermediate in size between the

428   smaller *Leptorhynchos elegans* and the larger *Caenagnathus collinsi*.

429   Evidence from the mandible is important for distinguishing DPF caenagnathids. Despite

430   being the most completely known caenagnathid from the DPF, the lack of definitive mandibular

431   material for *Chirostenotes pergracilis* has made it difficult to refer isolated specimens to this

432   taxon, and has left its synonymy with *Caenagnathus collinsi* ambiguous (Sues 1997). The

433   mandibles of CMN 8776 (*Caenagnathus collinsi*) are clearly distinct from all other mandibles

434   collected from the DPF and their taxonomic distinction is unambiguous. Two morphotypes can

435   be distinguished in the remaining mandibles from the DPF, but the taxa to which they pertain is

436   unclear. All of these mandibles have dentaries that are upturned at their anterior ends, but some

437   of the smaller specimens (e.g. TMP 1992.036.0390) have dentaries that are more strongly

438   upturned, have a more square anteroventral margin in lateral view, and have more widely

439   diverging rami in dorsal view (Currie et al. 1993; Longrich et al. 2013). Funston et al. (2019)

440   showed that these morphotypes differed in adult body size, and therefore likely pertained to two

441   different taxa: the larger *Chirostenotes pergracilis* and the smaller *Leptorhynchos elegans*.

442   However, this conclusion was tentative because neither *Chirostenotes pergracilis* nor

443   *Leptorhynchos elegans* are known from unambiguous mandibular material.

444   The discovery of UALVP 59400 is thus particularly important because it preserves a

445   relatively complete mandible in association with other postcranial bones. The morphology of the

446 mandible of UALVP 59400 shows that it is distinct from *Caenagnathus collinsi*, which lacks the

447 upturned anterior tip of the beak present in UALVP 59400. The dentaries of UALVP 59400 are

448 much larger than the small, histologically mature dentaries (UALVP 55639) described by

449 Funston et al. (2019), and are more similar in size and morphology to the largest dentaries in that

450 study (TMP 1992.036.1237). The correspondence in size, morphology, and histological signals

451 in TMP 1992.036.1237 (Gregory F. Funston et al. 2019) and UALVP 59400 strongly support the

452 referral of all this material to the same taxon. In this light, the isolated distal tarsal IV of UALVP

453 59400 is important. The lack of fusion between distal tarsal IV and the metatarsus—despite

454 histological maturity (see below)—shows that this specimen is distinct from *Leptorhynchos*

455 *elegans*, where the distal tarsals fuse to each other and the metatarsus at or before maturity (G.

456 Funston unpubl. diss.). Fusion of the hindlimb bones also appears to coincide with histological

457 maturity in other oviraptorosaurs (Gregory F. Funston et al. 2019). There is variation in the

458 ontogenetic sequence of some early theropods (C. T. Griffin & Nesbitt 2016; Christopher T.

459 Griffin & Nesbitt 2016; Griffin 2018), particularly regarding the fusion of the tarsometatarsus

460 (Griffin 2018). However, this variation is lost in more derived non-avian theropods, and is

461 virtually absent in avian theropods (Christopher T. Griffin & Nesbitt 2016). The close

462 phylogenetic position of caenagnathids to Aves suggests they probably had low variation in their

463 ontogenetic sequences, and thus the onset of fusion of the tarsometatarsus is unlikely to have

464 been highly variable through ontogeny. Indeed, in oviraptorosaurs with fused tarsometatarsi,

465 there appears to be minimal size variation in fused specimens of each taxon (Funston, Currie, &

466 Burns 2016; Funston, Currie, Eberth, et al. 2016; Gregory F. Funston et al. 2019), which

467 tentatively suggests that fusion coincides with the achievement of maximum body size. The

468 distinction of UALVP 59400 and, thus, the larger mandible morphotype from *Leptorhynchos*

469 *elegans* strongly supports the conclusion of Funston et al. (2019) that the larger mandible

470 morphotype is referable to *Chirostenotes pergracilis*.

471   Therefore, considering that 1) UALVP 59400 is distinct from *Caenagnathus collinsi* on

472 the basis of the mandible; 2) UALVP 59400 is separate from *Leptorhynchos elegans* on the basis

473 of the unfused distal tarsal IV; and 3) there is no evidence for a second caenagnathid taxon

474 intermediate in size between *Caenagnathus collinsi* and *Leptorhynchos elegans* in the Dinosaur

475 Park Formation; it can be concluded that UALVP 59400 is referable to *Chirostenotes*

476 *pergracilis*. A corollary of this is that, considering that 1) the smaller, upturned dentaries are

477 distinct from both *Caenagnathus collinsi* (CMN 8776) and *Chirostenotes pergracilis* (UALVP

478 59400); and 2) there is no evidence for a second, small caenagnathid in the Dinosaur Park

479 Formation; the small, upturned dentary morphotype represents *Leptorhynchos elegans*. The

480 further discovery of associated caenagnathid skeletons and the systematic osteohistological

481 sampling of material may provide new lines of evidence to refute or support these hypotheses.

482

483 *Anatomy:*

484 The referral of new material to *Chirostenotes pergracilis* fills important gaps in the anatomy of

485 this taxon. Referral of a relatively complete mandible (UALVP 59400) allows for more confident

486 identification of isolated mandibular material, including TMP 2001.012.0012, an exceptionally

487 complete mandible (Funston and Currie 2014). The ventral suture present on the surangular of

488 both these specimens is noteworthy. Comparison to *Citipati osmolskae* (Clark et al. 2002), an

489 undescribed *Conchoraptor gracilis,* and *Rinchenia mongoliensis* (Funston et al. 2018) shows that

490 this suture corresponds in position to the suture between the coronoid and surangular of

491 oviraptorids. This suggests that the coronoid is indeed present in caenagnathids, but is fused into

492   the ASC complex, as suspected by Currie et al. (1993). Combined with its presence in

493   *Incisivosaurus gauthieri* (Balanoff et al. 2009), this suggests that the coronoid is present

494   throughout Oviraptorosauria, but may appear absent because it fuses to the surangular.

495   UALVP 59400 includes cervical vertebrae, which have not yet been recovered from the

496   DPF, as well as a series of articulated caudal vertebrae, which may be useful for future

497   comparisons and referrals of isolated vertebrae. The cervical vertebrae are generally similar to

498   those of *Anzu wyliei* (Lamanna et al. 2014), *Apatoraptor pennatus* (Funston & Currie 2016) and

499   *Epichirostenotes curriei* (Sues 1997) in the reduced neural spines and anterodorsally directed

500   prezygapophyses. However, they differ from those of *Apatoraptor pennatus* in the better

501   development of the laminae connecting the postzygapophysis and transverse process, in which

502   respect they are more similar to *Epichirostenotes curriei* (Funston & Currie 2016). Similarly, the

503   cervical ribs appear unfused, despite the advanced skeletal maturity of UALVP 59400, which is

504   more like *Epichirostenotes curriei* than *Anzu wyliei* or *Apatoraptor pennatus* (Sues 1997;

505   Lamanna et al. 2014; Funston & Currie 2016). Compared to oviraptorids, the epipophyses of

506   caenagnathids are reduced, whereas in oviraptorids they are generally large anteriorly (Funston

507   et al. 2018). The caudal vertebrae of UALVP 59400 are similar to those of other oviraptorosaurs,

508   but the chevrons are distinctive. In oviraptorids, the chevrons are dorsoventrally deep

509   proximally, but become platelike, dorsoventrally shorter, and anteroposteriorly longer towards

510   the distal end of the tail (Balanoff & Norell 2012; Persons IV et al. 2013). Those of *Anzu wyliei*,

511   *Chirostenotes pergracilis*, and *Nomingia gobiensis*, in contrast, are much shorter in dorsoventral

512   height, and become rectangular toward the distal end of the tail (RZNCHEN Barsbold et al.

513   2000; Lamanna et al. 2014). The anteroposteriorly elongate proximal end of each chevron in

514   *Chirostenotes pergracilis* is distinctive among caenagnathids, but whether it served a functional

515   purpose is unclear.

516   The unusual stains and carbonaceous material preserved with the cervical vertebrae of

517   UALVP 59400 (Fig. 3C–E) are similar to features described in the feathers of oviraptorosaurs

518   and other theropods from China (Qiang et al. 1998; Xu & Zhang 2005; Xu et al. 2010; Xu et al.

519   2012; Xu et al. 2017). In particular, the filamentous, 'tufted' appearance of the stains and the

520   consistent orientation of the filaments parallel to the neck are similar to feather impressions on

521   the neck and back of *Anchiornis huxleyi* (Zheng et al. 2018), *Caudipteryx zoui* (Qiang et al.

522   1998), and *Sinosauropteryx prima* (Chen et al. 1998; Currie & Chen 2001; Smithwick, Nicholls,

523   et al. 2017). Considering that evidence of feather preservation is known from other specimens in

524   the Dinosaur Park and nearby Horseshoe Canyon Formations (Zelenitsky et al. 2012; van der

525   Reest et al. 2016), this seems a plausible explanation for these structures. Although some authors

526   have argued that these types of impressions represent collagen or the dermis (Lingham-Soliar et

527   al. 2007; Lingham-Soliar 2016), this interpretation is doubtful (Smithwick, Mayr, et al. 2017). In

528   any case, the filaments in UALVP 59400 are poorly preserved, probably as a result of

529   taphonomic degradation, and they provide little information about the type or distribution of

530   feathers in *Chirostenotes pergracilis*. Some possible branching structures can be detected (Fig.

531   3E), but none of these is conclusive and therefore whether these feathers are filaments or

532   pennaceous is ambiguous, although pennaceous feathers are known in other oviraptorosaurs

533   (Qiang et al. 1998; Xu et al. 2010). More information about the feathers in UALVP 59400 might

534   be gleaned by future chemical or microscopic analyses, which are outside of the scope of this

535   study.

536   The other isolated specimens described here overlap with TMP 1979.020.0001 but reveal

537   more of the morphology of those elements. Re-examination of a pathological tarsometatarsus

538   (TMP 1993.036.0181) previously referred to *Leptorhynchos elegans* suggests that it more likely

539   represents *Chirostenotes pergracilis*, because it lacks fusion of the distal tarsals to each other or

540   the metatarsals. Although less complete than the metatarsals of TMP 1979.020.0001, the

541   uncrushed nature of this specimen provides additional information on the pedal structure of

542   *Chirostenotes pergracilis*. Importantly, this specimen elucidates the morphology of the

543   proximodorsal process of distal tarsal IV, which is similar to—but smaller than—that of

544   *Elmisaurus elegans* (Osmólska 1981; Currie et al. 2016) and *Leptorhynchos elegans* (Funston,

545   Currie, & Burns 2016); it was probably a shared feature of most caenagnathids. The isolated

546   ilium (TMP 2002.012.0103) provides a second example of the unusually tall ilium of

547   *Chirostenotes pergracilis*, which is similar to that of *Rinchenia mongoliensis* (Funston et al.

548   2018). This specimen also shows that the inclination of the ventral edge of the pubic peduncle

549   may be useful for identifying more fragmentary ilia.

550   More of the anatomy and skeletal proportions of *Chirostenotes pergracilis* can be

551   reconstructed based on TMP 1979.020.0001 and UALVP 59400 (Fig. 1B). This shows that the

552   hindlimbs were exceptionally elongate, and the pelvis was relatively small. The tail was also

553   relatively short, and the shorter chevrons would have reduced space available for musculature.

554   Together with the elongate pedal digits adapted for grasping (Varricchio 2001; Longrich et al.

555   2010; Longrich et al. 2013), these features support previous suggestions that the hindlimbs of

556   *Chirostenotes pergracilis* were elongated to facilitate wading behaviour, rather than enhanced

557   cursoriality.

558

Growth in **Chirostenotes pergracilis***:*

559

560   The fragmentary nature of the sampled material limits the scope of the conclusions that can be

561   drawn. Regardless, the osteohistology of UALVP 59400 shows that this individual was

562   approaching maximum body size, and that growth had slowed considerably in the final years of

563   life. Assuming that doublet LAGs represent a single growth mark, UALVP 59400 was at least 9

564   years of age at death. There is some evidence of shape change or cortical drift preserved in the

565   cortex. For example, tighter curvature of the innermost LAG and its intersection with the

566   medullary cavity indicates that this region of the bone changed in curvature throughout life.

567   Reticular to sub-plexiform vascularity in the inner cortex of the femur or tibia of UALVP

568   59400 (Fig. 11) suggests that this individual had relatively rapid rates of growth at this stage of

569   life. This is similar to the outer cortex of UALVP 57349, a small caenagnathid tibia from the

570   HCF (Funston & Currie 2018), and to the bone in young avimimids (Gregory F. Funston et al.

571   2019). The same is true as well of ornithomimids (Varricchio et al. 2008; Cullen et al. 2014;

572   Skutschas et al. 2016), but appears not to have been the case in smaller non-theropods like

573   alvarezsaurs and dromaeosaurs (Erickson et al. 2009; Xu et al. 2018). These animals appear to

574   have had lower growth rates throughout life, reflected by their smaller body sizes (Erickson et al.

575   2009). Despite similar body sizes, the reticular–plexiform vascular patterns in UALVP 59400

576   and other caenagnathids (Funston & Currie 2018) suggest a more rapid growth rate than in

577   oviraptorids (Erickson et al. 2007; Norell et al. 2018), which have femoral cortices with

578   predominantly longitudinal vasculature. However, this may be the result of variation in element-

579   specific growth rate (Horner et al. 1999; Cullen et al. 2014; Woodward et al. 2014), reflecting

580   allometry rather than growth rates in the whole individual. Systematic sampling of caenagnathids

581 and oviraptorids of varying body sizes, controlling for sampling location, could clarify growth

582 rate variation in Oviraptorosauria.

583   Towards the periosteal surface of the cortex of UALVP 59400, the spacing between

584 CGMs is drastically reduced (Fig. 11E). This suggests that there was a transition to a slower

585 growth rate, and that this individual had approached maximum body size. Although variation in

586 LAG spacing between skeletal elements can pose problems for extrapolating maturity in isolated

587 specimens (Cullen et al. 2014), the high number of closely-spaced LAGs in UALVP 59400

588 strongly suggests that growth was diminished for several years, which is more likely to represent

589 skeletal maturity than allometry. Indeed, the parallel-fibered bone at the periosteal surface may

590 be indicative of an incipient EFS, signalling the cessation of growth. In extant amniotes, the

591 onset of sexual maturity coincides with a stark decrease in linear growth rates (Castanet et al.

592 2004; Lee & Werning 2008; Köhler et al. 2012; Botha-Brink et al. 2016). Although a broader

593 sample of caenagnathids would be required to be certain, the transition preserved in UALVP

594 59400 may indicate that this individual was sexually mature.

595

596 **Conclusions:**

597

598 A new partial skeleton referable to *Chirostenotes pergracilis* improves the skeletal representation

599 of this taxon. The specimen preserves the first mandible associated with postcrania from the

600 Dinosaur Park Formation, as well as the first cervical vertebrae and chevrons. Osteohistology

601 shows that the individual represented by UALVP 59400 was skeletally mature and approaching

602 maximum body size. Based on UALVP 59400, *Chirostenotes pergracilis* can be distinguished

603 from *Caenagnathus collinsi* on the basis of the dentary, which is anteriorly upturned, and from

604   *Leptorhynchos elegans* by its larger adult body size and the absence of fusion of the distal tarsals

605   and proximal metatarsals. This helps to clarify the taxonomy of Dinosaur Park Formation

606   caenagnathids, and mandibular material can now be confidently referred to each of the three

607   taxa.

608

609

610   **Acknowledgments:**

611

622

623   **Declaration of interests:**

624   The authors declare there are no conflicts of interest, financial or otherwise.

625

626   **References:**

627 Balanoff AM, Norell MA. 2012. Osteology of *Khaan mckennai* (Oviraptorosauria: Theropoda).
628 Bull Am Mus Nat Hist. 372:1–77.

629 Balanoff AM, Xu X, Kobayashi Y, Matsufune Y, Norell MA. 2009. Cranial Osteology of the
630 Theropod Dinosaur *Incisivosaurus gauthieri* (Theropoda: Oviraptorosauria). Am Mus Novit.
631 3651:1–35.

632 Barsbold R. 1976. On the evolution and systematics of the late Mesozoic carnivorous dinosaurs
633 [in Russian]. Paleontol Biostratigrafiâ Mongolii Tr Sovmest Sov Paleontol Èksped. 3:68–75.

634 Barsbold Rinchen, Currie PJ, Myhrvold NP, Osmólska H, Tsogtbaatar K, Watabe M. 2000. A
635 pygostyle from a non-avian theropod. Nature. 403(6766):155–156.

636 Barsbold RZNCHEN, Osmólska H, Watabe M, Currie PJ, Tsogtbaatar K. 2000. A new
637 oviraptorosaur [Dinosauria, Theropoda] from Mongolia: the first dinosaur with a pygostyle. Acta
638 Palaeontol Pol. 45(2):97–106.

639 Bell PR, Currie PJ, Russell DA. 2015. Large caenagnathids (Dinosauria, Oviraptorosauria) from
640 the uppermost Cretaceous of western Canada. Cretac Res. 52:101–107.

641 Botha-Brink J, Codron D, Huttenlocker AK, Angielczyk KD, Ruta M. 2016. Breeding Young as
642 a Survival Strategy during Earth's Greatest Mass Extinction. Sci Rep [Internet]. [accessed 2019
643 May 7] 6(1). http://www.nature.com/articles/srep24053

644 Castanet J, Croci S, Aujard F, Perret M, Cubo J, de Margerie E. 2004. Lines of arrested growth
645 in bone and age estimation in a small primate: Microcebus murinus. J Zool. 263(1):31–39.

646 Castanet J, Francillon-Vieillot H, Meunier FJ, de Ricqlès AJ. 1990. Bone and individual aging.
647 In: Hall BK, editor. Bone. Boca Raton, Florida: CRC Press; p. 245–284.

648 Chen P, Dong Z, Zhen S. 1998. An exceptionally well-preserved theropod dinosaur from the
649 Yixian Formation of China. Nature. 391(6663):147–152.

650 Clark JM, Norell MA, Rowe T. 2002. Cranial anatomy of *Citipati osmolskae* (Theropoda,
651 Oviraptorosauria), and a reinterpretation of the holotype of *Oviraptor philoceratops*. Am Mus
652 Novit.:1–24.

653 Cullen TM, Evans DC, Ryan MJ, Currie PJ, Kobayashi Y. 2014. Osteohistological variation in
654 growth marks and osteocyte lacunar density in a theropod dinosaur (Coelurosauria:
655 Ornithomimidae). BMC Evol Biol. 14(1):231.

656 Currie PJ, Funston GF, Osmolska H. 2016. New specimens of the crested theropod dinosaur
657 *Elmisaurus rarus* from Mongolia. Acta Palaeontol Pol. 61(1):143–157.

658 Currie PJ. 1989. The first records of *Elmisaurus* (Saurischia, Theropoda) from North America.
659 Can J Earth Sci. 26(6):1319–1324.

660   Currie PJ, Chen P. 2001. Anatomy of <i>Sinosauropteryx prima</i> from Liaoning,
661   northeastern China. Can J Earth Sci. 38(12):1705–1727.

662   Currie PJ, Godfrey SJ, Nessov L. 1993. New caenagnathid (Dinosauria: Theropoda) specimens
663   from the Upper Cretaceous of North America and Asia. Can J Earth Sci. 30:2255–2272.

664   Currie PJ, Russell DA. 1988. Osteology and relationships of *Chirostenotes pergracilis*
665   (Saurischia, Theropoda) from the Judith River (Oldman) Formation of Alberta, Canada. Can J
666   Earth Sci. 25(7):972–986.

667   Erickson GM, Curry Rogers K, Varricchio DJ, Norell MA, Xu X. 2007. Growth patterns in
668   brooding dinosaurs reveals the timing of sexual maturity in non-avian dinosaurs and genesis of
669   the avian condition. Biol Lett. 3(5):558–561.

670   Erickson GM, Rauhut OWM, Zhou Z, Turner AH, Inouye BD, Hu D, Norell MA. 2009. Was
671   Dinosaurian Physiology Inherited by Birds? Reconciling Slow Growth in Archaeopteryx.DeSalle
672   R, editor. PLoS ONE. 4(10):e7390.

673   Francillon-Vieillot H, de Buffrenil V, Castanet J, Gkraudie J, Meunier FJ, Sire JY, Zylberberg L,
674   de Ricqlès AJ. 1990. Microstructure and Mineralization of Vertebrate Skeletal Tissues. In: Carter
675   JG, editor. Skelet Biominer Patterns Process Evol Trneds. New York: Van Nostrand Reinhold; p.
676   471–530.

677   Funston GF, Currie PJ. 2014. A previously undescribed caenagnathid mandible from the late
678   Campanian of Alberta, and insights into the diet of *Chirostenotes pergracilis* (Dinosauria:
679   Oviraptorosauria). Can J Earth Sci. 51(2):156–165.

680   Funston GF, Currie PJ. 2016. A new caenagnathid (Dinosauria: Oviraptorosauria) from the
681   Horseshoe Canyon Formation of Alberta, Canada, and a reevaluation of the relationships of
682   Caenagnathidae. J Vertebr Paleontol. 36(4):e1160910.

683   Funston GF, Currie PJ. 2018. A small caenagnathid tibia from the Horseshoe Canyon Formation
684   (Maastrichtian): Implications for growth and lifestyle in oviraptorosaurs. Cretac Res. 92:220–
685   230.

686   Funston GF, Currie PJ, Burns M. 2016. New elmisaurine specimens from North America and
687   their relationship to the Mongolian *Elmisaurus rarus*. Acta Palaeontol Pol. 61(1):159–173.

688   Funston GF, Currie PJ, Eberth DA, Ryan MJ, Chinzorig T, Badamgarav D, Longrich NR. 2016.
689   The first oviraptorosaur (Dinosauria: Theropoda) bonebed: evidence of gregarious behaviour in a
690   maniraptoran theropod. Sci Rep. 6:35782.

691   Funston Gregory F., Currie PJ, Ryan MJ, Dong Z-M. 2019. Birdlike growth and mixed-age
692   flocks in avimimids (Theropoda, Oviraptorosauria). Sci Rep. 9(1):18816.

693   Funston Gregory F., Mendonca SE, Currie PJ, Barsbold R. 2018. Oviraptorosaur anatomy,
694   diversity and ecology in the Nemegt Basin. Palaeogeogr Palaeoclimatol Palaeoecol [Internet].
695   [accessed 2017 Dec 4]. http://linkinghub.elsevier.com/retrieve/pii/S0031018217306065

696 Funston GF, Persons WS, Bradley GJ, Currie PJ. 2015. New material of the large-bodied
697 caenagnathid *Caenagnathus collinsi* from the Dinosaur Park Formation of Alberta, Canada.
698 Cretac Res. 54:179–187.

699 Funston Gregory F., Wilkinson RD, Simon DJ, Leblanc AH, Wosik M, Currie PJ. 2019.
700 Histology of Caenagnathid (Theropoda, Oviraptorosauria) Dentaries and Implications for
701 Development, Ontogenetic Edentulism, and Taxonomy. Anat Rec.(doi:10.1002/ar.24205):1–17.

702 Gauthier J. 1986. Saurischian monophyly and the origin of birds. In: Padian K, editor. Orig Birds
703 Evol Flight. Vol. 8. San Francisco, California: California Academy of Sciences; p. 1–55.

704 Gilmore CW. 1924. A new coelurid dinosaur from the Belly River Cretaceous of Alberta. Can
705 Geol Surv Bull. 38:1–12.

706 Griffin CT. 2018. Developmental patterns and variation among early theropods. J Anat.
707 232(4):604–640.

708 Griffin C. T., Nesbitt SJ. 2016. The femoral ontogeny and long bone histology of the Middle
709 Triassic (?late Anisian) dinosauriform *Asilisaurus kongwe* and implications for the growth of
710 early dinosaurs. J Vertebr Paleontol. 36(3):e1111224.

711 Griffin Christopher T., Nesbitt SJ. 2016. Anomalously high variation in postnatal development is
712 ancestral for dinosaurs but lost in birds. Proc Natl Acad Sci. 113(51):14757–14762.

713 Horner JR, Padian K. 2004. Age and growth dynamics of *Tyrannosaurus rex*. Proc R Soc B Biol
714 Sci. 271(1551):1875–1880.

715 Horner JR, Padian K, de Ricqlès A. 2001. Comparative osteohistology of some embryonic and
716 perinatal archosaurs: developmental and behavioral implications for dinosaurs. Paleobiology.
717 27(1):39–58.

718 Horner JR, de Ricqlès A, Padian K. 1999. Variation in dinosaur skeletochronology indicators:
719 implications for age assessment and physiology. Paleobiology. 25(3):295–304.

720 Huene F. 1914. The dinosaurs not a natural order. Am J Sci. 38:145–146.

721 Köhler M, Marín-Moratalla N, Jordana X, Aanes R. 2012. Seasonal bone growth and physiology
722 in endotherms shed light on dinosaur physiology. Nature. 487(7407):358–361.

723 Lamanna MC, Sues H-D, Schachner ER, Lyson TR. 2014. A New Large-Bodied
724 Oviraptorosaurian Theropod Dinosaur from the Latest Cretaceous of Western North America.
725 PLoS ONE. 9(3):e92022.

726 Lee AH, O'Connor PM. 2013. Bone histology confirms determinate growth and small body size
727 in the noasaurid theropod *Masiakasaurus knopfleri*. J Vertebr Paleontol. 33(4):865–876.

728 Lee AH, Werning S. 2008. Sexual maturity in growing dinosaurs does not fit reptilian growth
729 models. Proc Natl Acad Sci. 105(2):582–587.

730   Lingham-Soliar T. 2016. A densely feathered ornithomimid (Dinosauria: Theropoda) from the
731   Upper Cretaceous Dinosaur Park Formation, Alberta, Canada: A comment. Cretac Res. 62:86–
732   89.

733   Lingham-Soliar T, Feduccia A, Wang X. 2007. A new Chinese specimen indicates that
734   'protofeathers' in the Early Cretaceous theropod dinosaur *Sinosauropteryx* are degraded collagen
735   fibres. Proc R Soc B Biol Sci. 274(1620):1823–1829.

736   Longrich NR, Barnes K, Clark S, Millar L. 2013. Caenagnathidae from the Upper Campanian
737   Aguja Formation of West Texas, and a Revision of the Caenagnathinae. Bull Peabody Mus Nat
738   Hist. 54(1):23–49.

739   Longrich NR, Currie PJ, Zhi-Ming D. 2010. A new oviraptorid (Dinosauria: Theropoda) from
740   the Upper Cretaceous of Bayan Mandahu, Inner Mongolia. Palaeontology. 53(5):945–960.

741   Ma W, Wang J, Pittman M, Tan Q, Tan L, Guo B, Xu X. 2017. Functional anatomy of a giant
742   toothless mandible from a bird-like dinosaur: *Gigantoraptor* and the evolution of the
743   oviraptorosaurian jaw. Sci Rep. 7(1):10.1038/s41598-017-15709–7.

744   de Margerie E. 2004. Assessing a relationship between bone microstructure and growth rate: a
745   fluorescent labelling study in the king penguin chick (Aptenodytes patagonicus). J Exp Biol.
746   207(5):869–879.

747   Marsh OC. 1881. Classification of the Dinosauria. Am J Sci. 23:81–86.

748   Norell MA, Balanoff AM, Barta DE, Erickson GM. 2018. A Second Specimen of *Citipati*
749   *Osmolskae* Associated With a Nest of Eggs from Ukhaa Tolgod, Omnogov Aimag, Mongolia.
750   Am Mus Novit. 3899(3899):1–44.

751   Osmólska H. 1976. New light on the skull anatomy and systematic position of *Oviraptor*. Nature.
752   262:683–684.

753   Osmólska H. 1981. Coossified tarsometatarsi in theropod dinosaurs and their bearing on the
754   problem of bird origins. Palaeontol Pol. 42:79–95.

755   Owen R. 1842. Report on British fossil reptiles. Part II. Rep Br Assoc Adv Sci. 11:60–204.

756   Padian K, Lamm E-T, Werning S. 2013. Selection of Specimens. In: Padian K, Lamm E-T,
757   editors. Bone Histol Foss Tetrapods Adv Methods Anal Interpret. Berkeley, California:
758   University of California Press; p. 35–54.

759   Parks WA. 1933. New species of dinosaurs and turtles from the Upper Cretaceous Formations of
760   Alberta. Univ Tor Stud Geol Ser. 34:1–24.

761   Persons IV WS, Currie PJ, Norell MA. 2013. Oviraptorosaur tail forms and functions. Acta
762   Palaeontol Pol. 59(3):553–567.

763 Pu H, Zelenitsky DK, Lü J, Currie PJ, Carpenter K, Xu L, Koppelhus EB, Jia S, Xiao L, Chuang
764 H, et al. 2017. Perinate and eggs of a giant caenagnathid dinosaur from the Late Cretaceous of
765 central China. Nat Commun. 8:14952.

766 Qiang J, Currie PJ, Norell MA, Shu-An J. 1998. Two feathered dinosaurs from northeastern
767 China. Nature. 393(6687):753–761.

768 van der Reest AJ, Wolfe AP, Currie PJ. 2016. A densely feathered ornithomimid (Dinosauria:
769 Theropoda) from the Upper Cretaceous Dinosaur Park Formation, Alberta, Canada. Cretac Res.
770 58:108–117.

771 Seeley HG. 1888. On the classification of the fossil animals commonly named Dinosauria. Proc
772 R Soc Lond. 43(258–265):161–171.

773 Skutschas PP, Boitsova EA, Averianov AO, Sues H-D. 2016. Ontogenetic changes in long-bone
774 histology of an ornithomimid theropod dinosaur from the Upper Cretaceous Bissekty Formation
775 of Uzbekistan. Hist Biol.:1–15.

776 Smithwick FM, Mayr G, Saitta ET, Benton MJ, Vinther J. 2017. On the purported presence of
777 fossilized collagen fibres in an ichthyosaur and a theropod dinosaur.Smith A, editor.
778 Palaeontology. 60(3):409–422.

779 Smithwick FM, Nicholls R, Cuthill IC, Vinther J. 2017. Countershading and Stripes in the
780 Theropod Dinosaur Sinosauropteryx Reveal Heterogeneous Habitats in the Early Cretaceous
781 Jehol Biota. Curr Biol. 27(21):3337-3343.e2.

782 Stein KWH, Werner J. 2013. Preliminary Analysis of Osteocyte Lacunar Density in Long Bones
783 of Tetrapods: All Measures Are Bigger in Sauropod Dinosaurs.Evans DC, editor. PLoS ONE.
784 8(10):e77109.

785 Sternberg CM. 1932. Two new theropod dinosaurs from the Belly River Formation of Alberta.
786 Can Field-Nat. 46(5):99–105.

787 Sternberg CM. 1934. Notes on certain recently described dinosaurs. Can Field-Nat. 48:7–8.

788 Sternberg RM. 1940. A toothless bird from the Cretaceous of Alberta. J Paleontol. 14(1):81–85.

789 Sues H-D. 1997. On *Chirostenotes*, a Late Cretaceous oviraptorosaur (Dinosauria: Theropoda)
790 from western North America. J Vertebr Paleontol. 17(4):698–716.

791 Sues H-D, Averianov A. 2015. New material of *Caenagnathasia martinsoni* (Dinosauria:
792 Theropoda: Oviraptorosauria) from the Bissekty Formation (Upper Cretaceous: Turonian) of
793 Uzbekistan. Cretac Res. 54:50–59.

794 Sullivan RM, Jasinski SE, Van Tomme MPA. 2011. A new caenagnathid *Ojoraptorsaurus*
795 *boerei*, n. gen., n. sp (Dinosauria, Oviraptorosauria), from the Upper Ojo Alamo Formation
796 (Naashoibito Member), San Juan Basin, New Mexico. N M Mus Nat Hist Sci Bull. 53(3):418–
797 428.

798   Tsuihiji T, Watabe M, Barsbold R, Tsogtbaatar K. 2015. A gigantic caenagnathid
799   oviraptorosaurian (Dinosauria: Theropoda) from the Upper Cretaceous of the Gobi Desert,
800   Mongolia. Cretac Res. 56:60–65.

801   Tsuihiji T, Watabe M, Tsogtbaatar K, Barsbold R. 2016. Dentaries of a caenagnathid
802   (Dinosauria: Theropoda) from the Nemegt Formation of the Gobi Desert in Mongolia. Cretac
803   Res. 63:148–153.

804   Varricchio DJ. 1993. Bone microstructure of the Upper Cretaceous theropod dinosaur *Troodon*
805   *formosus*. J Vertebr Paleontol. 13(1):99–104.

806   Varricchio DJ. 2001. Late Cretaceous Oviraptorosaur (Theropoda) Dinosaurs from Montana. In:
807   Tanke DH, Carpenter K, editors. Mesoz Vertebr Life. Bloomington: Indiana University Press; p.
808   42–57.

809   Varricchio DJ, Sereno PC, Xijin Z, Lin T, Wilson JA, Lyon GH. 2008. Mud-Trapped Herd
810   Captures Evidence of Distinctive Dinosaur Sociality. Acta Palaeontol Pol. 53(4):567–578.

811   Wang S, Stiegler J, Wu P, Chuong C-M, Hu D, Balanoff A, Zhou Y, Xu X. 2017. Heterochronic
812   truncation of odontogenesis in theropod dinosaurs provides insight into the macroevolution of
813   avian beaks. Proc Natl Acad Sci. 114(41):10930–10935.

814   Wang S, Zhang Q, Yang R. 2018. Reevaluation of the Dentary Structures of Caenagnathid
815   Oviraptorosaurs (Dinosauria, Theropoda). Sci Rep. 8(1):10.1038/s41598-017-18703–1.

816   Woodward HN, Freedman Fowler EA, Farlow JO, Horner JR. 2015. *Maiasaura*, a model
817   organism for extinct vertebrate population biology: a large sample statistical assessment of
818   growth dynamics and survivorship. Paleobiology. 41(04):503–527.

819   Woodward HN, Horner JR, Farlow JO. 2014. Quantification of intraskeletal histovariability in
820   *Alligator mississippiensis* and implications for vertebrate osteohistology. PeerJ. 2:e422.

821   Xu X, Choiniere J, Tan Q, Benson RBJ, Clark J, Sullivan C, Zhao Q, Han F, Ma Q, He Y, et al.
822   2018. Two Early Cretaceous Fossils Document Transitional Stages in Alvarezsaurian Dinosaur
823   Evolution. Curr Biol. 28(17):2853-2860.e3.

824   Xu X, Currie P, Pittman M, Xing L, Meng Q, Lü J, Hu D, Yu C. 2017. Mosaic evolution in an
825   asymmetrically feathered troodontid dinosaur with transitional features. Nat Commun. 8:14972.

826   Xu X, Tan Q, Wang J, Zhao X, Tan L. 2007. A gigantic bird-like dinosaur from the Late
827   Cretaceous of China. Nature. 447:844–847.

828   Xu X, Wang K, Zhang K, Ma Q, Xing L, Sullivan C, Hu D, Cheng S, Wang S. 2012. A gigantic
829   feathered dinosaur from the Lower Cretaceous of China. Nature. 484(7392):92–95.

830   Xu X, Zhang F. 2005. A new maniraptoran dinosaur from China with long feathers on the
831   metatarsus. Naturwissenschaften. 92(4):173–177.

832 Xu X, Zheng X, You H. 2010. Exceptional dinosaur fossils show ontogenetic development of
833 early feathers. Nature. 464(7293):1338–1341.

834 Yao X, Wang X-L, Sullivan C, WANG S, Stidham T, Xu X. 2015. *Caenagnathasia* sp.
835 (Theropoda: Oviraptorosauria) from the Iren Dabasu Formation (Upper Cretaceous: Campanian)
836 of Erenhot, Nei Mongol, China. Vertebr Palasiat. 53(4):291–298.

837 Yu Y, Wang K, Chen S, Sullivan C, Wang S, Wang P, Xu X. 2018. A new caenagnathid
838 dinosaur from the Upper Cretaceous Wangshi Group of Shandong, China, with comments on
839 size variation among oviraptorosaurs. Sci Rep. 8(1):10.1038/s41598-018-23252–2.

840 Zanno LE, Tucker RT, Canoville A, Avrahami HM, Gates TA, Makovicky PJ. 2019. Diminutive
841 fleet-footed tyrannosauroid narrows the 70-million-year gap in the North American fossil record.
842 Commun Biol [Internet]. [accessed 2019 Sep 16] 2(1). http://www.nature.com/articles/s42003-
843 019-0308-7

844 Zelenitsky DK, Therrien F, Erickson GM, DeBuhr CL, Kobayashi Y, Eberth DA, Hadfield F.
845 2012. Feathered Non-Avian Dinosaurs from North America Provide Insight into Wing Origins.
846 Science. 338(6106):510–514.

847 Zheng X, Wang X, Sullivan C, Zhang X, Zhang F, Wang Y, Li F, Xu X. 2018. Exceptional
848 dinosaur fossils reveal early origin of avian-style digestion. Sci Rep. 8(1):14217.

849

850

851 Table 1. Selected measurements of UALVP 59400 and other caenagnathids

Measurement (mm)		*Chirostenotes pergracilis*		*Apatoraptor pennatus*	*Epichirostenotes curriei*	*Anzu wyliei*	*Nomingia gobiensis*
		UALVP 59400	TMP 2001.012.0012	TMP 1993.051.0001	ROM 43250	CM 78001	MPC-D 100/119
Mandible: length of articular ridge		23.5	24.7	21.1	-	35.7	-
Mandible: minimum height of dentary		20.7	20.9	13.6	-	25.8	-
Cervical Vertebrae (length of centrum)	Cv7	49e	-	54.5	81	86	-
	Cv8	57e	-	55	85	95	-
Caudal Vertebrae (length of centrum)	C8	27.1	-	-	-	34	22
	C9	25.2	-	-	-	32	21
	C10	22.3	-	-	-	31	20
	C11	21.4	-	-	-	31	18
	C12	19.5	-	-	-	-	18
	C13	19.4	-	-	-	-	16
	C14	16.1	-	-	-	-	16
	C15	20.4	-	-	-	-	16
	C16	20.9	-	-	-	-	17
	C17	16.9	-	-	-	-	19
Chevron 8, length		58.7	-	-	-	-	42

852

853

854
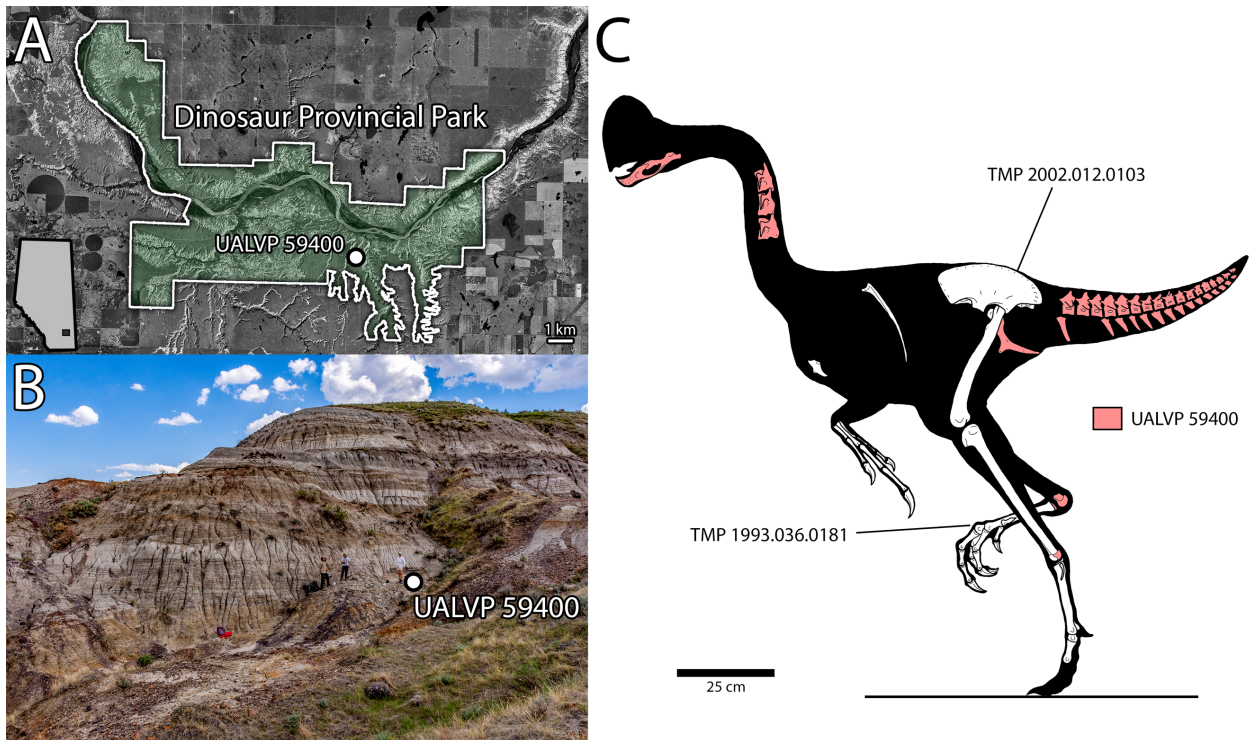
857 FIGURE 1. **A,** Satellite image of Dinosaur Provincial Park (highlighted in green), showing the

858 locality where UALVP 59400 was found. Inset shows location of satellite image within Alberta,

859 Canada. **B**, Field photography of site, indicated by the white point. Note three people standing to

860 the left of the point, for scale. **C**, Reconstruction of *Chirostenotes pergracilis*, showing known

861 elements, with bones preserved in UALVP 59400 highlighted in red. Satellite imagery in (A)

862 from Google Maps (map data: © Google Maps), used under fair use terms.

863
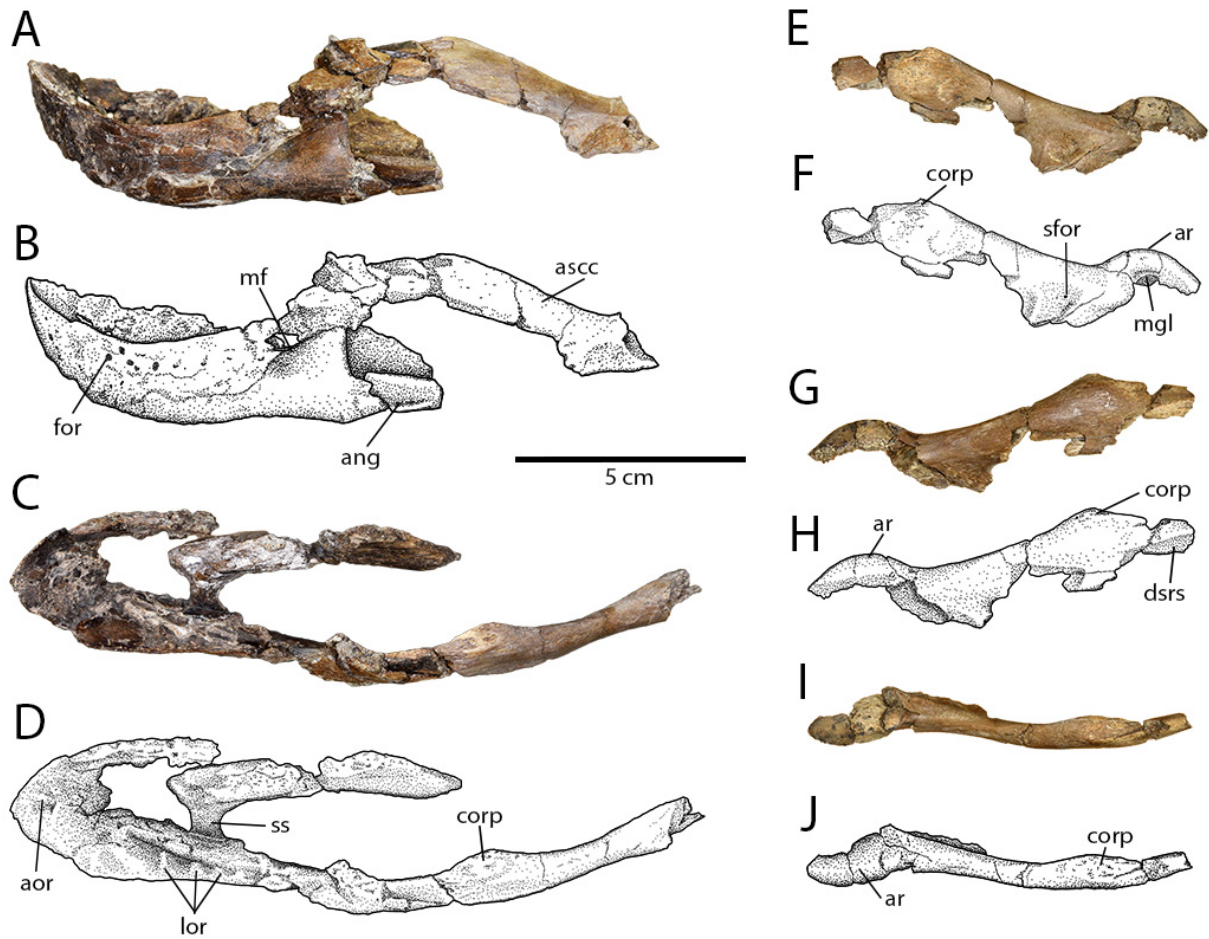
FIGURE 2. Mandibles of *Chirostenotes pergracilis* (UALVP 59400). **A, B**, Photograph (A) and illustration (B) of mandibles in left lateral view. **C, D,** Photograph (C) and illustration (D) of mandibles in dorsal view. **E, F,** Photograph (E) and illustration (F) of right articular-surangular-coronoid complex in medial view. **G, H,** Photograph (E) and illustration (F) of right articular-surangular-coronoid complex in lateral view. **I, J**, Photograph (I) and illustration (J) of right articular-surangular-coronoid complex in dorsal view. **Abbreviations: ang**, angular; **aor**, anterior occlusal ridge; **ar**, articular ridge; **ascc**, articular-surangular-coronoid complex; **corp**, coronoid process; **dsrs**, dentary-surangular suture; **for**, foramen; **lor**, lateral occlusal ridges; **mf**, mandibular fossa; **mgl**, medial glenoid; **sfor**, surangular foramen; **ss**, symphyseal sulcus.

38
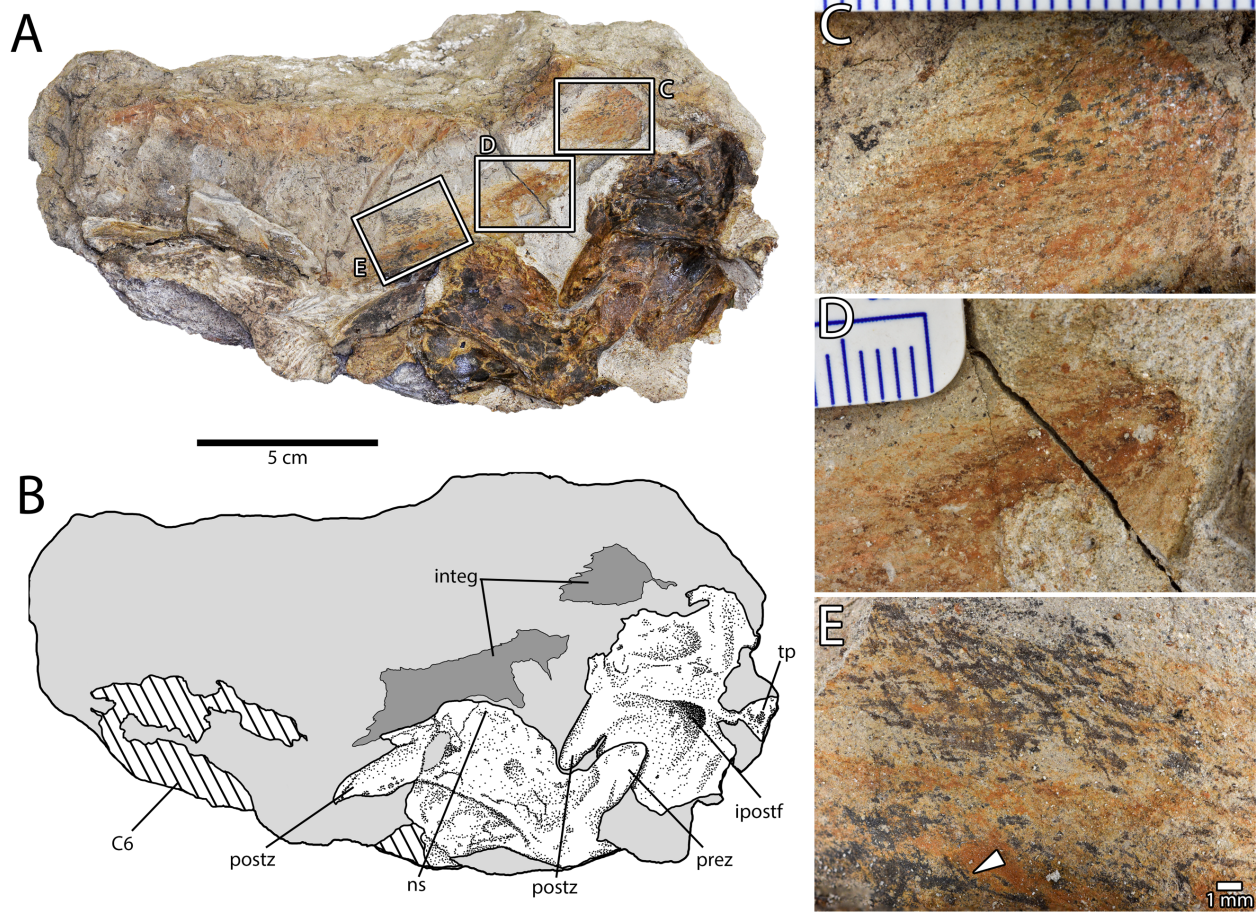
877 FIGURE 3. Cervical vertebrae of *Chirostenotes pergracilis* (UALVP 59400). **A, B,** Photograph

878 (A) and illustration (B) of postaxial cervical vertebrae four, five, and six in right lateral view.

879 Boxes in (A) indicate the locations of close-up images (C–E). Light grey indicates matrix, dark

880 grey indicates possible integument, and lines indicate broken bone. **C–E,** Close-up photographs

881 of possible feather impressions dorsal to the cervical vertebrae. Note the filamentous impressions

882 and the consistent orientation of the fibers. Arrow in (E) indicates possible branching structure.

883 Scales in (C) and (D) are in millimetres. **Abbreviations: C6**, postaxial cervical vertebra six;

884 **integ**, possible integumentary structures; **ipostf**, infrapostzygapophyseal fossa; **ns**, neural spine;

885 **postz**, postzygapophysis; **prez**, prezygapophysis; **tp**, transverse process.

886

887
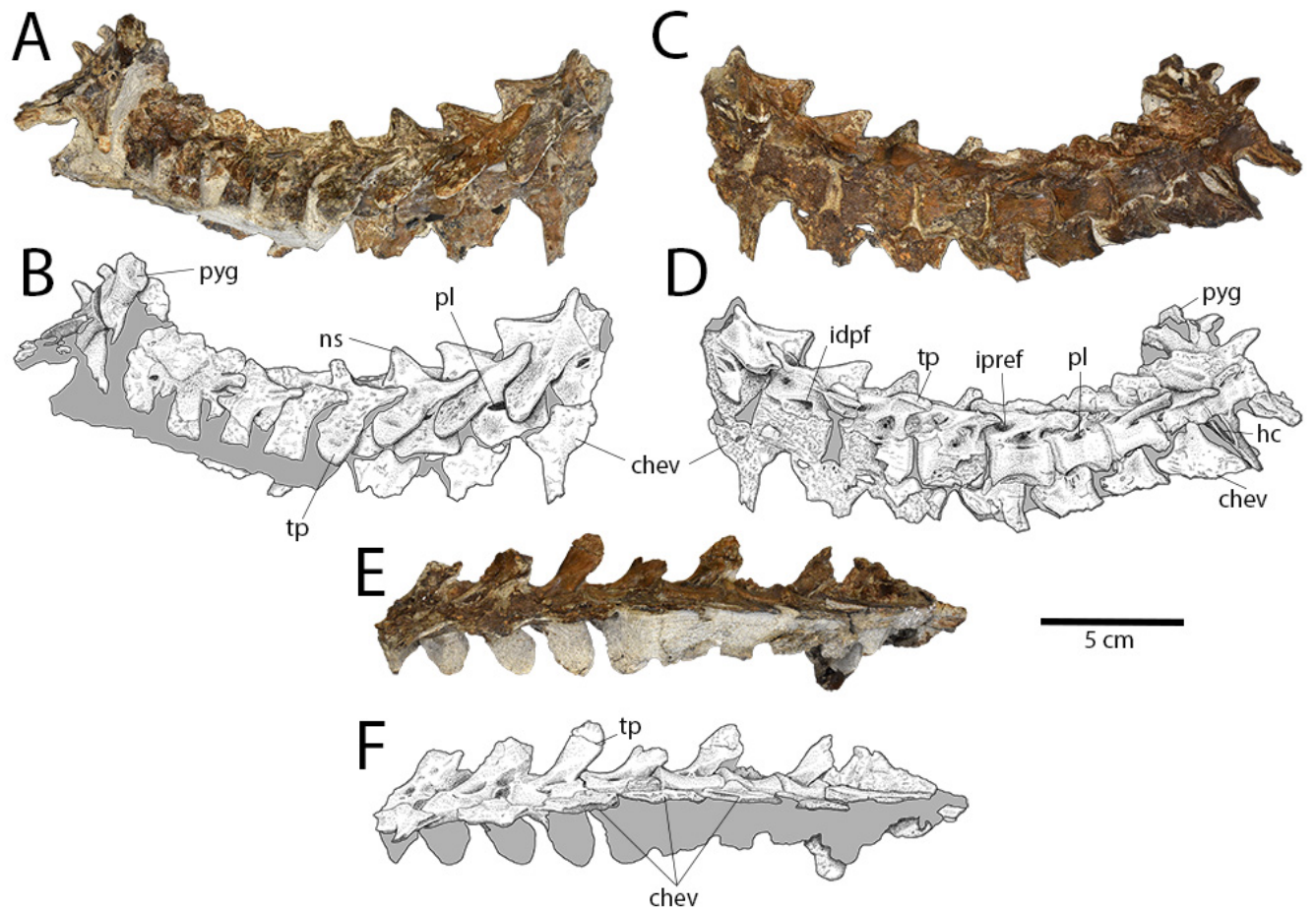
FIGURE 4. Caudal vertebrae of *Chirostenotes pergracilis* (UALVP 59400). **A, B,** Photograph

(A) and illustration (B) of articulated distal caudal vertebral series in right lateral view. **C, D,**

Photograph (C) and illustration (D) of articulated distal caudal vertebral series in left lateral

view. **E, F,** Photograph (E) and illustration (F) of articulated distal caudal vertebral series in

ventral view. **Abbreviations: chev**, chevron; **hc**, haemal canal; **idpf**, infradiapophyseal fossa;

ipref, infraprezygapophyseal fossa; **ns**, neural spine; **pl**, pleurocoel; **pyg**, pre-pygal vertebra; **tp**,

transverse process.

895

40
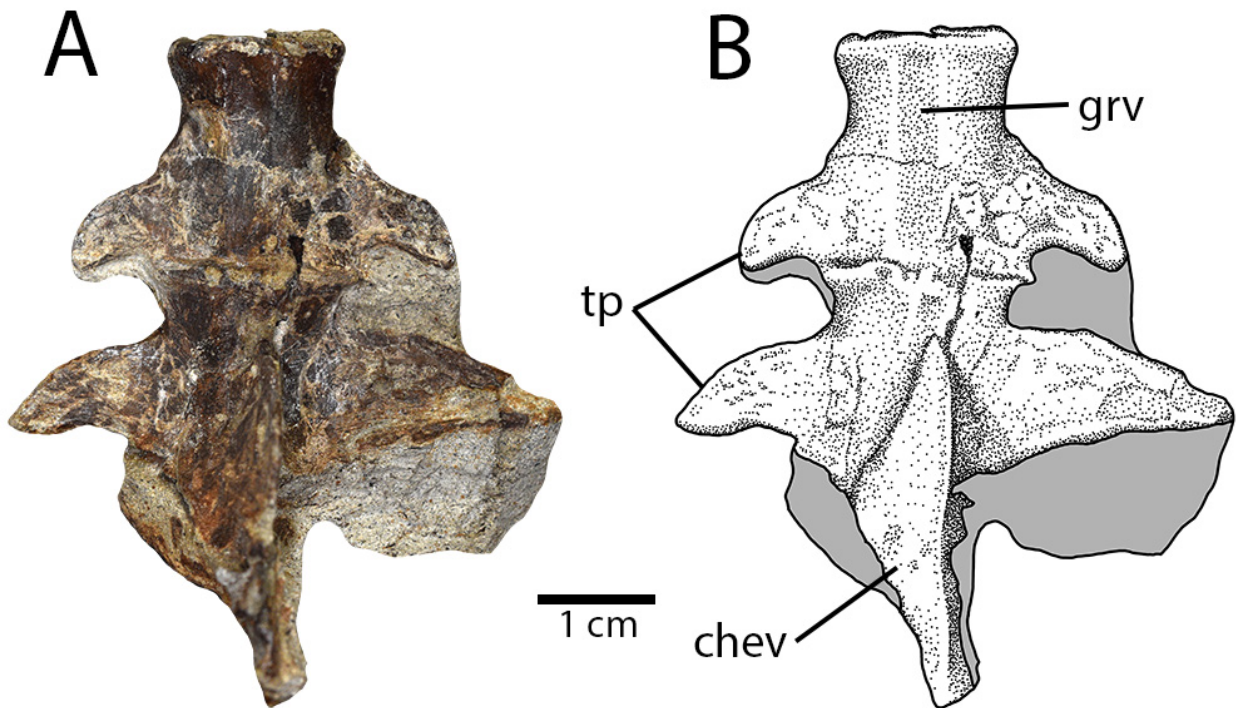
FIGURE 5. Distal caudal vertebrae of *Chirostenotes pergracilis* (UALVP 59400). **A, B,**
Photograph (A) and illustration (B) of pre-pygal caudal vertebrae of UALVP 59400 in ventral
view, showing anteriorly-directed transverse processes, midline ventral groove, and large,
platelike chevrons. Anterior is downwards, distal (posterior) is upwards, and lateral is to either
side. **Abbreviations: chev,** chevron; **grv**, groove; **tp**, transverse process.
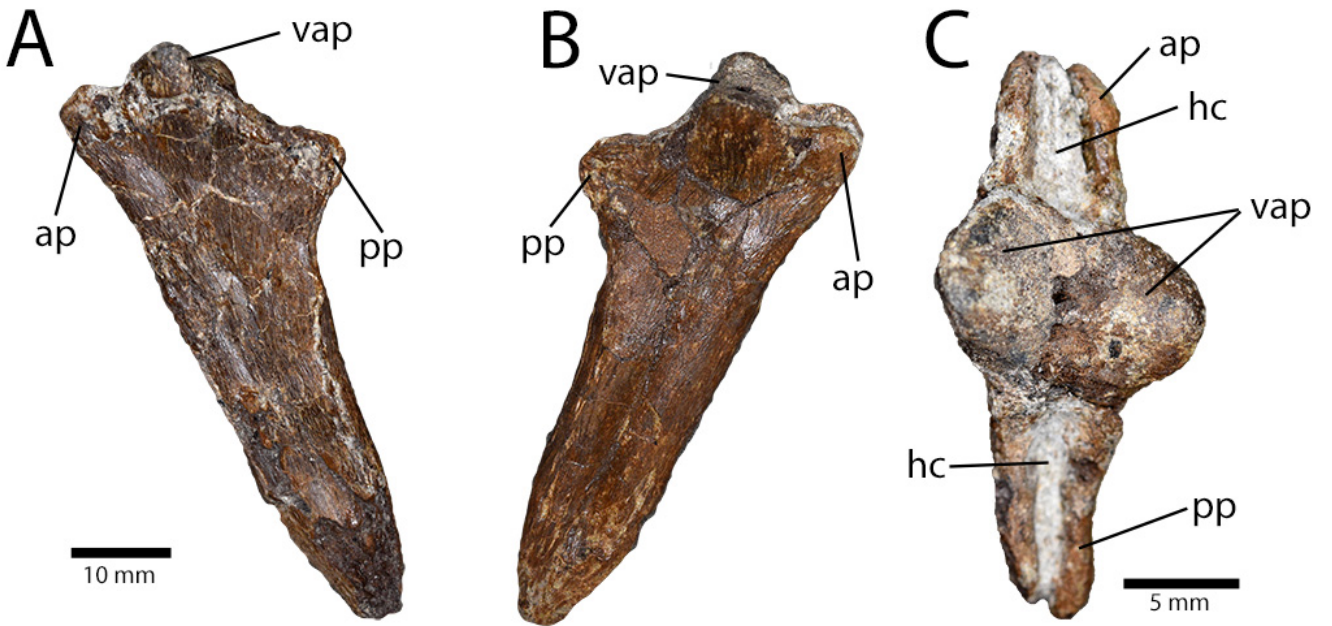
FIGURE 6. Chevron of *Chirostenotes pergracilis* (UALVP 59400). **A–C,** mid-caudal chevron in left lateral (A), right lateral (B), and proximal views. **Abbreviations: ap**, anterior process; **hc**, haemal canal; **pp**, posterior process ;**vap**, vertebral articular processes.
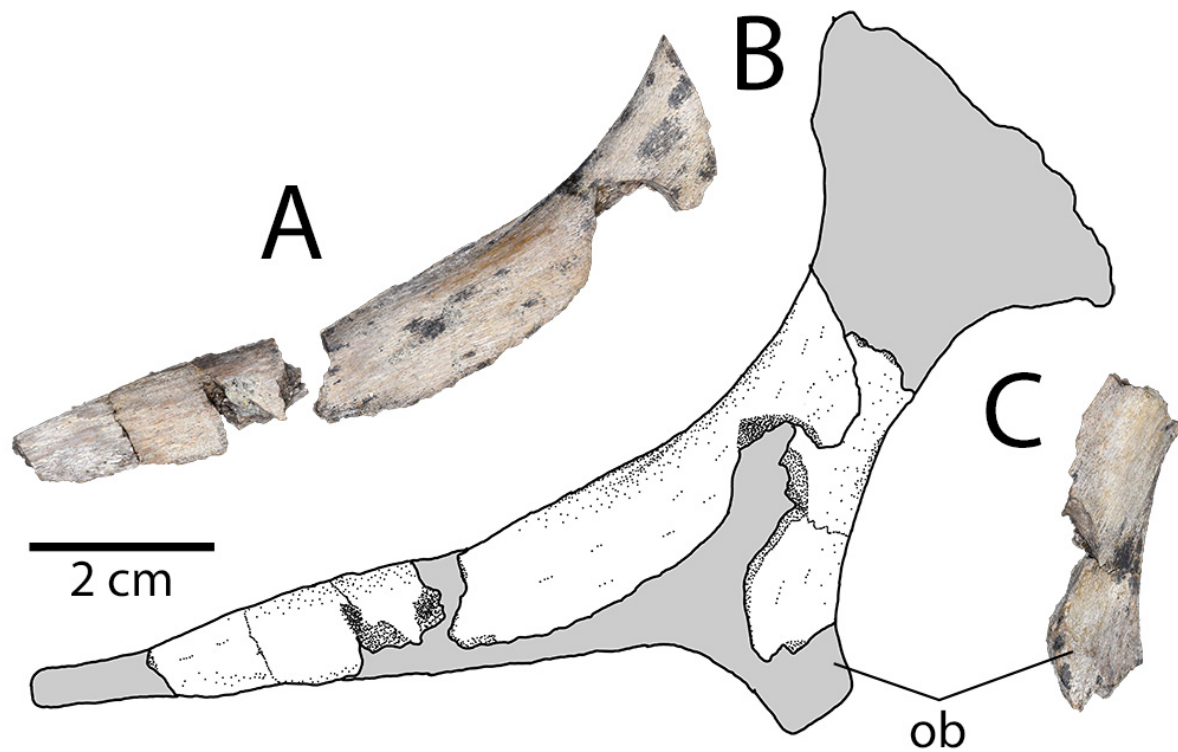
FIGURE 7. Ischium of *Chirostenotes pergracilis* (UALVP 59400). **A,** Fragments of right

ischium in lateral view. **B**, Composite reconstruction of ischium based on fragments of the left

and right ischia, reconstructed using the complete ischium of TMP 1979.020.0001 (silhouette).

C, Fragment of right ischium in medial view. **Abbreviation: ob**, obturator process.
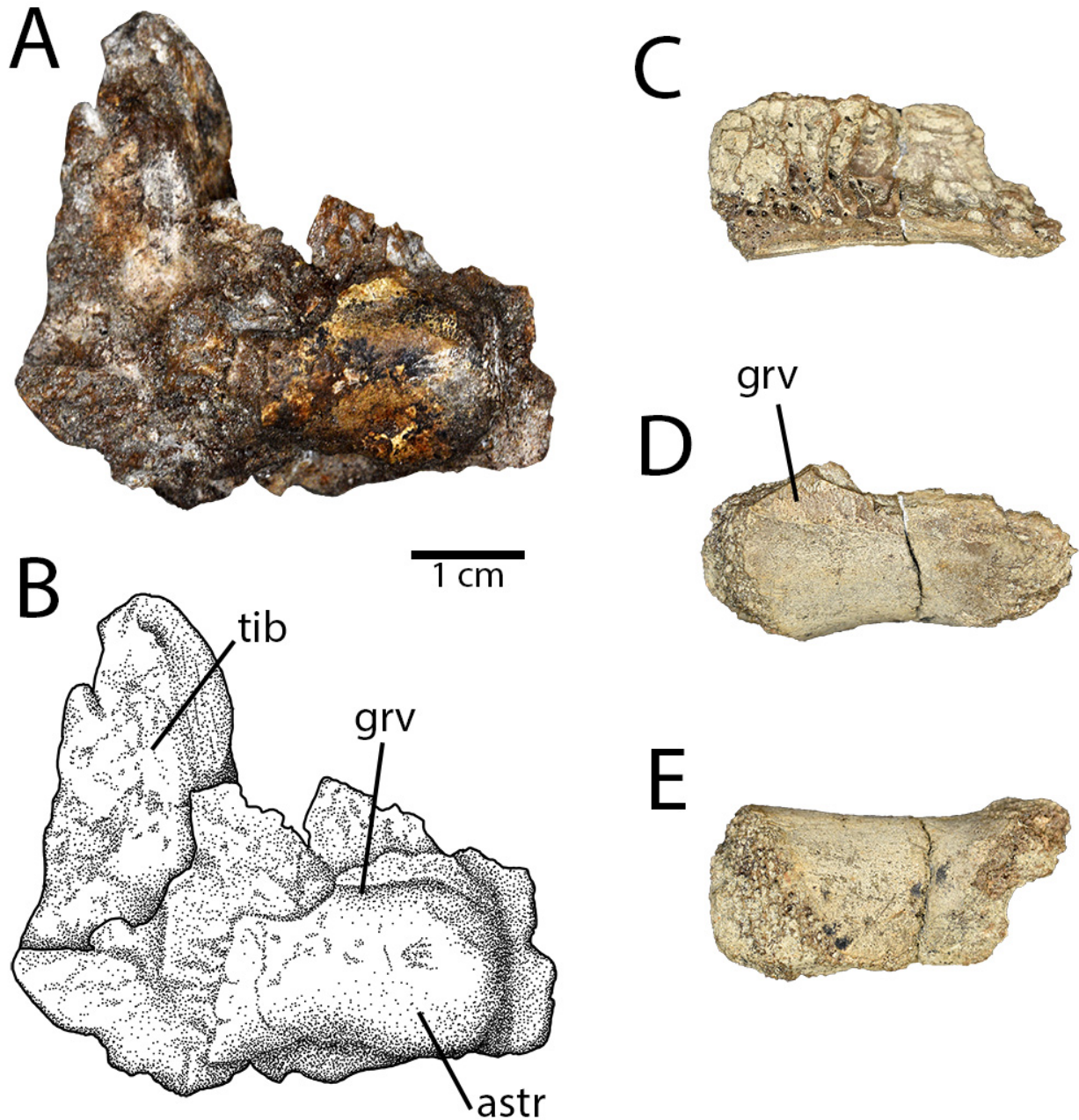
FIGURE 8. Astragalocalcanei of *Chirostenotes pergracilis* (UALVP 59400). **A, B,** Photograph (A) and illustration (B) of right distal tibia and astragalocalcaneum in anterior view. **C–E,** left astragalocalcaneum in dorsal (C), anterior (D), and ventral (E) views. **Abbreviations: astr,** astragalus; **grv**, groove; **tib**, tibia.
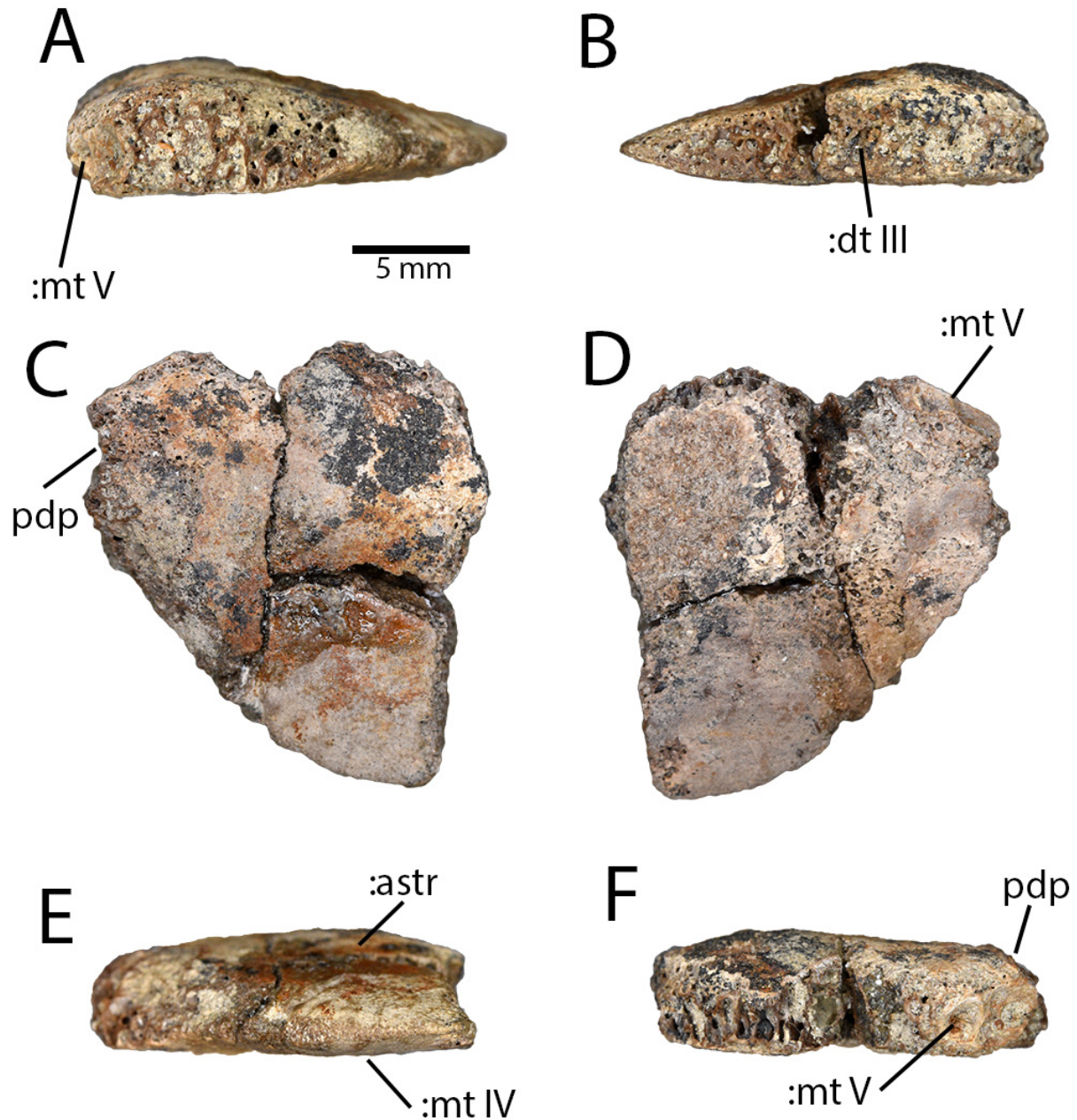
FIGURE 9. Distal tarsal IV of *Chirostenotes pergracilis* (UALVP 59400). **A–F**, Right distal tarsal IV in lateral (A), medial (B), proximal (C), distal (D), anterior (E) and posterior (F) views. Note the intact distal surface, indicating that the distal tarsal was not fused to the proximal end of metatarsal IV. **Abbreviations: :astr,** contact for astragalus; **:dt III**, contact for distal tarsal III;

928   **:mt IV**, contact for metatarsal IV; **:mt V**, contact for metatarsal V; **pdp**, base of proximodorsal

929   process.

930
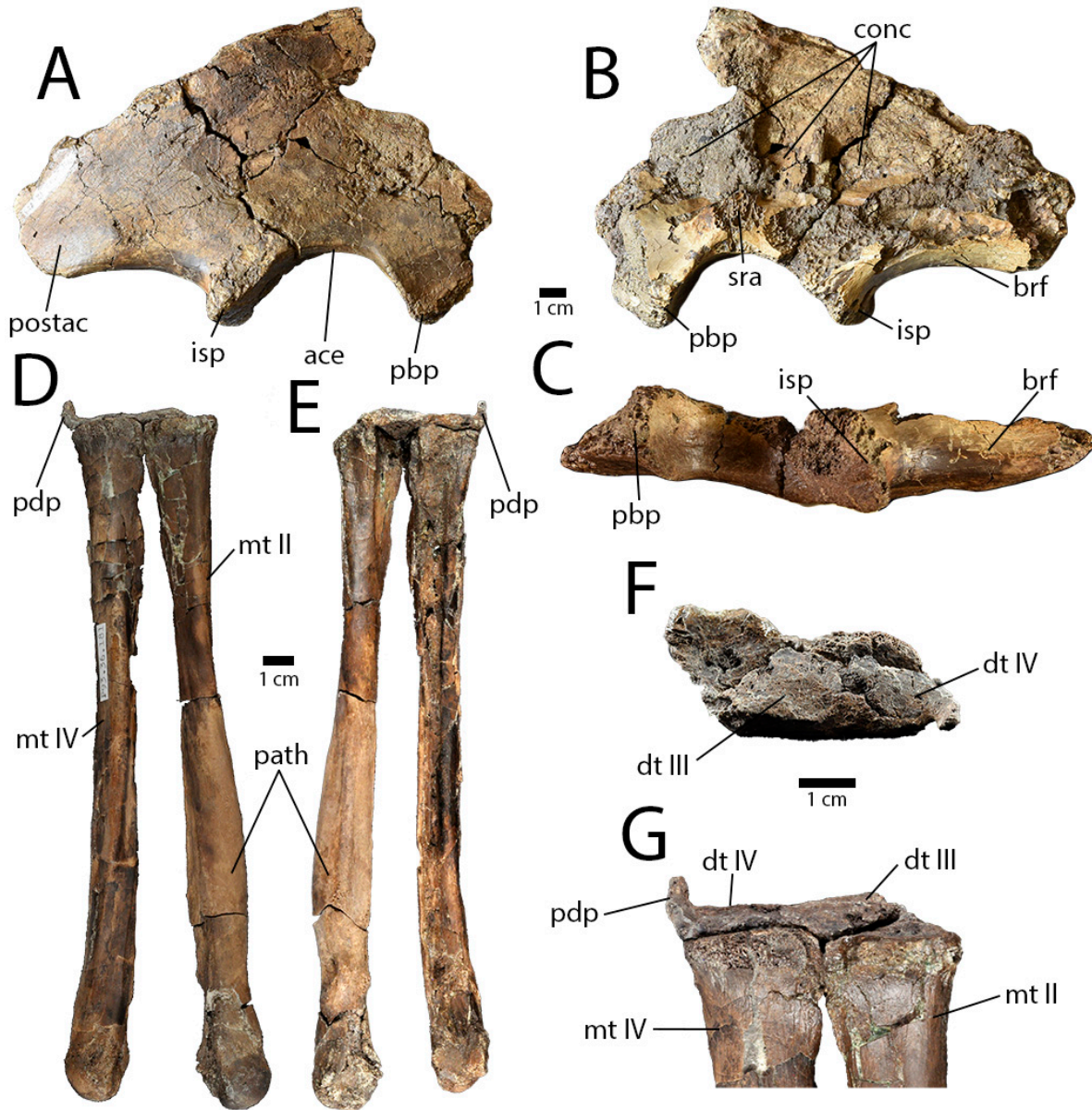
FIGURE 10. Other specimens referable to *Chirostenotes pergracilis* (TMP 2002.012.0103 and

TMP 1993.036.0181). **A–C,** Partial right ilium (TMP 2002.012.0103) in lateral (A), medial (B),

and ventral (C) views. **D–F,** Partial right tarsometatarsus (TMP 1993.036.0181) comprising

938   distal tarsals III and IV, and metatarsals II and IV in anterior (D), posterior (E), and proximal (F)

939   views. **G**, closeup of proximal end of partial right tarsometatarsus (TMP 1993.036.0181),

940   showing lack of fusion between metatarsals II and IV and between the distal tarsals and

941   metatarsals. **Abbreviations: : ace**, acetabulum; **antr**, anterior ridge; **brf**, brevis fossa; **dt III,**

942   distal tarsal III; **dt IV**, distal tarsal IV; ; **intf**, intermediate fossa; **isp**, ischiadic peduncle; **MT II,**

943   metatarsal II; **MT IV**, metatarsal IV; **path**, pathological region; **pbp**, pubic peduncle; **pdp**,

944   proximodorsal process; **postac,** postacetabular blade; **postf**, posterior fossa; **sra**, sacral rib

945   attachment.

946
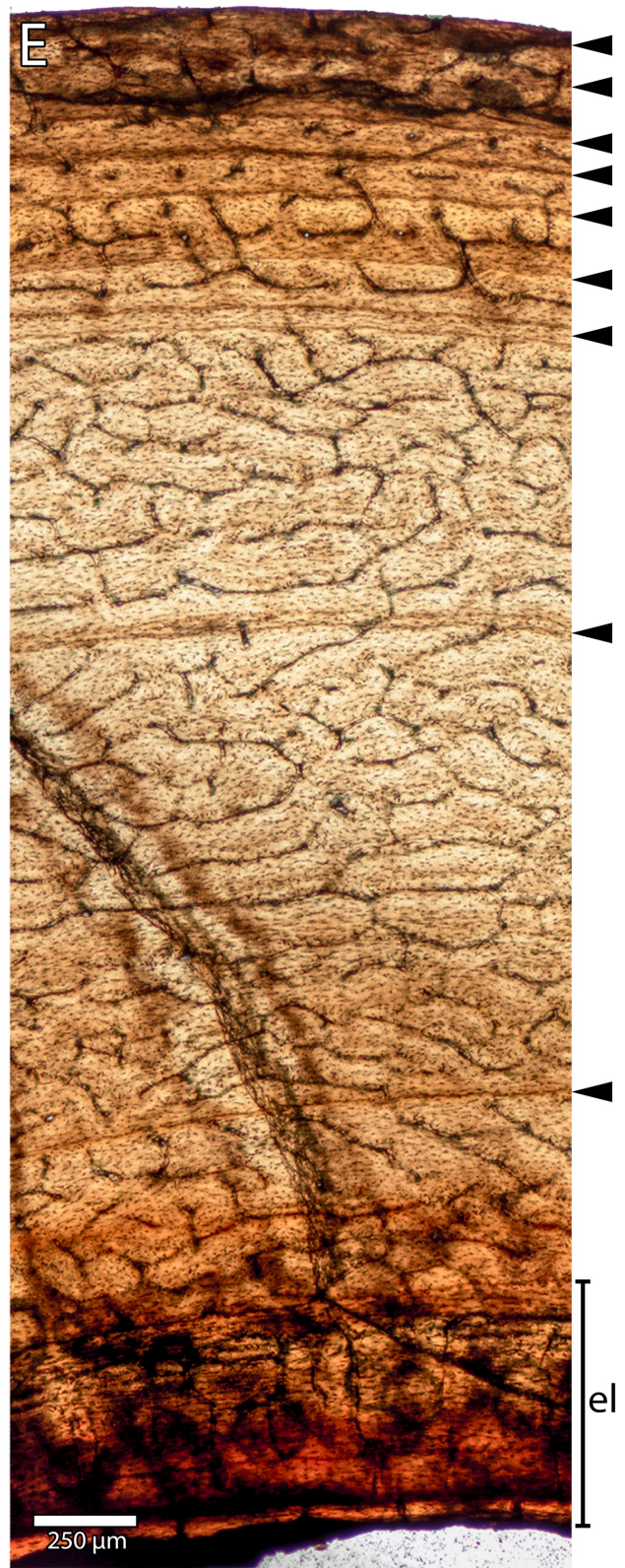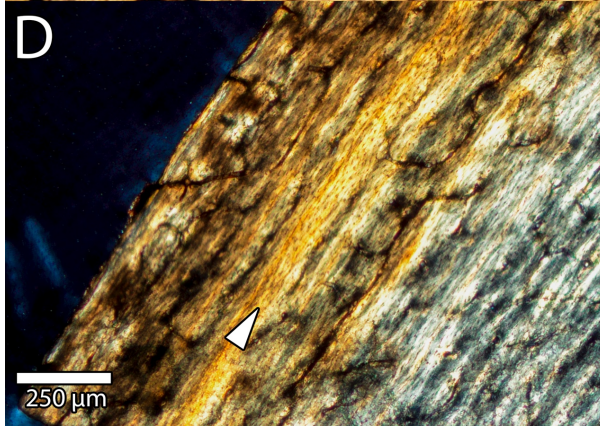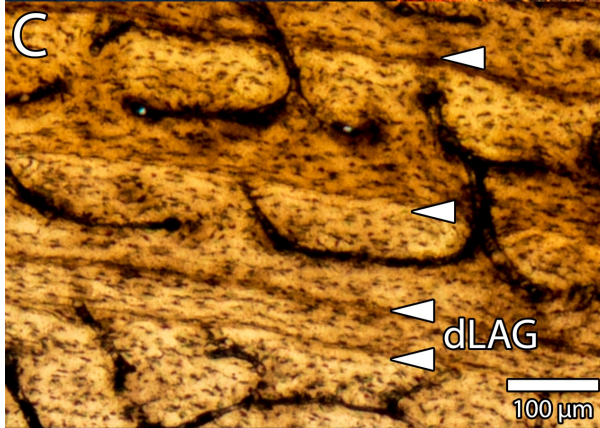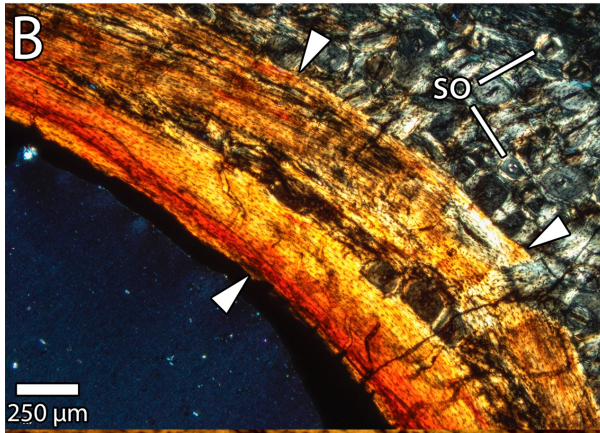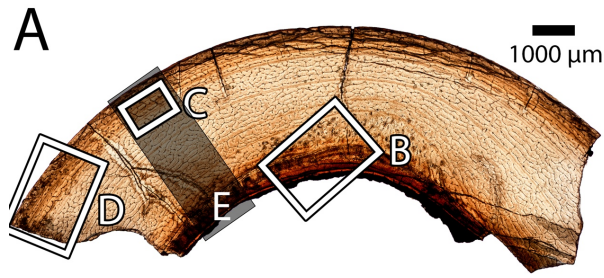
948

949 FIGURE 11. Osteohistology of *Chirostenotes pergracilis* (UALVP 59400). **A**, Transverse thin

950 section of long-bone fragment from UALVP 59400 under normal light, showing the locations of

951 other images. **B,** Detail of endosteal lamellae (arrows) and secondary remodeling along the

952 endosteal margin and inner cortex under cross-polarized light. **C**, Detail of lines of arrested

953 growth (arrows) in the outer cortex, showing doublet LAGs, under normal light. **D**, Detail of the

954 periosteal region of the cortex, showing a high proportion of parallel-fibered bone and an

955 annulus (arrow) associated with a line of arrested growth, under cross-polarized light. **E**, The

956 cortex of UALVP 59400, showing resorption by the medullary cavity and endosteal lamellae

957 (el), nine cyclical growth marks (arrows), and changes in the vascular pattern from reticular

958 endosteally to longitudinal periosteally. **Abbreviations: dLAG**, doublet lines of arrested growth;

959 **el**, endosteal lamellae; **so**, secondary osteon.

960

961

962   **Word count: 8447**